

The Resonant Drag Instability (RDI): Acoustic Modes

Philip F. Hopkins¹, & Jonathan Squire¹

¹TAPIR, Mailcode 350-17, California Institute of Technology, Pasadena, CA 91125, USA

Submitted to MNRAS, July 2017

ABSTRACT

Recently, Squire & Hopkins (2017) showed any coupled dust-gas mixture is subject to a class of linear “resonant drag instabilities” (RDI). These can drive large dust-to-gas ratio fluctuations even at arbitrarily small dust-to-gas mass ratios μ . Here, we explore the RDI in the simple case where the gas satisfies neutral hydrodynamics and supports acoustic waves ($\omega^2 = c_s^2 k^2$). The gas and dust are coupled via an arbitrary drag law and subject to external accelerations (e.g. gravity, radiation pressure). If there is any dust drift velocity, the system is unstable. The instabilities exist for *all* dust-to-gas ratios μ and their growth rates depend only weakly on μ , as $\sim \mu^{1/3}$. The behavior changes depending on whether the drift velocity is larger or smaller than the sound speed c_s . In the supersonic limit a “resonant” instability appears with growth rate increasing *without limit* with wavenumber, even for vanishingly small μ and values of the coupling strength (“stopping time”). In the subsonic limit instabilities always exist, but their growth rates no longer increase indefinitely towards small wavelengths. The results are robust to the drag law and equation-of-state of the gas. The instabilities directly drive exponentially growing dust-to-gas-ratio fluctuations, which can be large even when the modes are otherwise weak. We discuss physical implications for cool-star winds, AGN-driven winds and torii, and starburst winds: the instabilities alter the character of these outflows and will drive clumping and turbulence in both gas and dust.

Key words: instabilities — turbulence — ISM: kinematics and dynamics — star formation: general — galaxies: formation — cosmology: theory — planets and satellites: formation — accretion, accretion disks

1 INTRODUCTION

Astrophysical fluids are replete with dust, and the dynamics of the dust-gas mixture in these “dusty fluids” are critical to astrochemistry, star and planet formation, “feedback” from stars and active galactic nuclei (AGN) in galaxy formation, the origins and evolution heavy elements, cooling in the inter-stellar medium, stellar evolution in cool stars, and more. Dust is also ubiquitous as a source of extinction or contamination in almost all astrophysical contexts. As such, it is critical to understand how dust and gas interact, and whether these interactions produce phenomena that could segregate or produce novel dynamics or instabilities in the gas or dust.

Recently, Squire & Hopkins (2017) (henceforth SH) showed that there exists a general class of previously unrecognized instabilities of dust-gas mixtures. The SH “resonant drag instability” (RDI) generically appears whenever a gas system that supports some wave or linear perturbation mode (in the absence of dust) also contains dust moving with a finite drift velocity \mathbf{w}_s relative to the gas. The “resonance” is then between the phase velocity of the gas wave, and the dust drift velocity projected along the wavevector direction ($\mathbf{w}_s \cdot \hat{\mathbf{k}}$). Some previously well-studied instabilities – most notably the “streaming instability” of grains in protostellar disks (Youdin & Goodman 2005), which arises due to a resonance with the disk’s epicyclic oscillations – belong to the general RDI category. These instabilities *directly* generate fluctuations in the dust-to-gas ratio and the relative dynamics of the dust and gas, making them potentially critical for the host of phenomena above (see, e.g., Chiang & Youdin 2010 for applications of the disk streaming instability).

The relative dust-gas drift velocity \mathbf{w}_s and the ensuing instabilities can arise for a myriad of reasons. For example, in the photospheres of cool stars, in the interstellar medium of star-forming molecular clouds or galaxies, and in the obscuring “torus” or narrow-line region around an AGN, dust is accelerated by absorbed radiation from the stars/AGN, generating movement relative to the

gas. Similarly, in a proto-stellar disk, gas is supported via pressure, while grains (without such pressure) gradually sediment. In both cases, a drag force, which couples the dust to the gas, then causes the dust to accelerate the gas, or vice versa. While there has been an extensive literature on such mechanisms – e.g., radiation-pressure driven winds – there has been surprisingly little focus on the question of whether the dust can stably transfer momentum to gas under these conditions. We will argue that these process are all inherently unstable.

Perhaps the simplest example of the RDI occurs when one considers ideal, inviscid hydrodynamics, where the only wave (absent dust) is a sound wave. This “acoustic RDI” has not yet been studied, despite having potentially important implications for a wide variety of astrophysical systems. In this paper, we therefore explore this manifestation of the RDI in detail. We show that homogenous gas, coupled to dust via some drag law, is generically unstable to a spectrum of exponentially-growing linear instabilities (both resonant and non-resonant), regardless of the form of the dust drag law, the magnitude of the drift velocity, the dust-to-gas ratio, the drag coefficient or “stopping time,” and the source of the drift velocity. If the drift velocity exceeds the sound speed, the “resonance” condition is always met and the growth rate increases without limit at short wavelengths.

We present the basic derivation and linearized equations-of-motion in § 2, including various extensions and caveats. In § 3, we then derive the stability conditions, growth rates, and structure of the unstable modes for arbitrary drag laws, showing in § 4 how this specifies to various physical cases (Epstein drag, Stokes drag, and Coulomb drag). The discussion of § 3–§ 4 is necessarily rather involved, covering a variety of different unstable modes in different physical regimes, and the reader more interested in applications may wish to read just the general overview in § 3.1, the discussion of mode structure in § 3.9, and skim through relevant drag laws of § 4. We briefly discuss the non-linear regime (§ 5), scales where our

arXiv:1707.02997v1 [astro-ph.SR] 10 Jul 2017

analysis breaks down (§ 6), and the relation of these instabilities to those discussed in previous literature (§ 7), before considering applications to different astrophysical systems including cool-star winds, starbursts, AGN obscuring torii and narrow-line regions, and protoplanetary disks (§ 8). We conclude in § 9.

2 BASIC EQUATIONS & LINEAR PERTURBATIONS

2.1 General Case with Constant Streaming

Consider a mixture of gas and a second component which can be approximated as a pressure-free fluid (at least for *linear* perturbations; see Youdin & Goodman 2005 and App. A of Jacquet et al. 2011), interacting via some generalized drag law. We will refer to this second component as “dust” henceforth. For now we consider an ideal, inviscid gas, so the system is described by mass and momentum conservation for both fluids:

$$\begin{aligned} \frac{\partial \rho}{\partial t} + \nabla \cdot (\mathbf{u} \rho) &= 0, \\ \left(\frac{\partial}{\partial t} + \mathbf{u} \cdot \nabla \right) \mathbf{u} &= -\frac{\nabla P}{\rho} + \mathbf{g} + \frac{\rho_d}{\rho} \frac{(\mathbf{v} - \mathbf{u})}{t_s}, \\ \frac{\partial \rho_d}{\partial t} + \nabla \cdot (\mathbf{v} \rho_d) &= 0, \\ \left(\frac{\partial}{\partial t} + \mathbf{v} \cdot \nabla \right) \mathbf{v} &= -\frac{(\mathbf{v} - \mathbf{u})}{t_s} + \mathbf{g} + \mathbf{a}, \end{aligned} \quad (1)$$

where (ρ, \mathbf{u}) and (ρ_d, \mathbf{v}) are the density and velocity of the gas and dust, respectively; \mathbf{g} is the external acceleration of the gas while $\mathbf{g} + \mathbf{a}$ is the external acceleration of dust (i.e., \mathbf{a} is the difference in the dust and gas acceleration), and P is the gas pressure. The dust experiences a drag acceleration $\mathbf{a}_{\text{drag}} = -(\mathbf{v} - \mathbf{u})/t_s$ with an arbitrary drag coefficient t_s , known as the “stopping time” (which can be a function of other properties). The term in t_s in the gas acceleration equation is the “back-reaction” – its form is dictated by conservation of momentum.

The homogeneous solution to Eq. (1) is the dust and gas accelerating together at the same rate, with a constant relative drift velocity \mathbf{w}_s :

$$\begin{aligned} \rho^h &= \langle \rho \rangle = \rho_0, \\ \rho_d^h &= \langle \rho_d \rangle = \rho_{d,0} \equiv \mu \rho_0, \\ \mathbf{u}^h &= \langle \mathbf{u} \rangle = \mathbf{u}_0 + \left[\mathbf{g} + \mathbf{a} \left(\frac{\mu}{1 + \mu} \right) \right] t, \\ \mathbf{v}^h &= \langle \mathbf{v} \rangle = \langle \mathbf{u} \rangle + \mathbf{w}_s, \\ \mathbf{w}_s &\equiv \frac{\mathbf{a} \langle t_s \rangle}{1 + \mu} = \frac{\mathbf{a}^h(\rho^h, \mathbf{w}_s, \dots)}{1 + \mu}, \end{aligned} \quad (2)$$

where we define the total mass-ratio between the two fluids as $\mu \equiv \langle \rho_d \rangle / \langle \rho \rangle$, and $\langle t_s \rangle = t_s(\langle \rho \rangle, \langle \mathbf{v} \rangle, \dots)$ is the value of t_s for the homogeneous solution. Note that $\langle t_s \rangle$ can depend on \mathbf{w}_s , so Eq. (2) is in general a non-linear equation for \mathbf{w}_s . Let us also define the normalized drift speed $w_s \equiv |\mathbf{w}_s|/c_s$, where c_s is the usual sound speed ($c_s^2 \equiv \partial P / \partial \rho$); w_s is a key parameter in determining stability properties and will be used extensively below.

We now consider small perturbations δ : $\rho = \rho^h + \delta\rho$, $\mathbf{u} = \mathbf{u}^h + \delta\mathbf{u}$, etc., and adopt a free-falling frame moving with the ho-

mogeneous gas solution $\langle \mathbf{u} \rangle$. Linearizing Eq. (1), we obtain,

$$\begin{aligned} \frac{\partial \delta\rho}{\partial t} &= -\rho_0 \nabla \cdot \delta\mathbf{u}, \\ \frac{\partial \delta\mathbf{u}}{\partial t} &= -c_s^2 \frac{\nabla \delta\rho}{\rho_0} + \mu \frac{(\delta\mathbf{v} - \delta\mathbf{u})}{\langle t_s \rangle}, \\ &\quad - \mu \frac{\mathbf{w}_s}{\langle t_s \rangle} \left(\frac{\delta t_s}{\langle t_s \rangle} + \frac{\delta\rho}{\rho_0} - \frac{\delta\rho_d}{\mu\rho_0} \right), \\ \left(\frac{\partial}{\partial t} + \mathbf{w}_s \cdot \nabla \right) \delta\rho_d &= -\mu \rho_0 \nabla \cdot \delta\mathbf{v}, \\ \left(\frac{\partial}{\partial t} + \mathbf{w}_s \cdot \nabla \right) \delta\mathbf{v} &= -\frac{(\delta\mathbf{v} - \delta\mathbf{u})}{\langle t_s \rangle} + \frac{\mathbf{w}_s \delta t_s}{\langle t_s \rangle^2}, \end{aligned} \quad (3)$$

where we have defined δt_s as the linearized perturbation to t_s ; i.e. $t_s \equiv \langle t_s \rangle + \delta t_s(\delta\rho, \delta\mathbf{v}, \dots) + \mathcal{O}(\delta^2)$.

A couple important results are immediately clear: after removing the homogeneous solution, \mathbf{g} vanishes – an identical uniform acceleration on dust and gas produces no interesting behavior. If $\mathbf{a} = \mathbf{0}$, then $\mathbf{w}_s = \mathbf{0}$ and the equations become those for a coupled pair of soundwaves with friction (all modes are stable or decay). Likewise if $\delta\mathbf{u}$ and $\delta\mathbf{v}$ are strictly perpendicular to \mathbf{w}_s . Finally, the acceleration \mathbf{a} is important only insofar as it produces a non-vanishing dust-gas drift velocity \mathbf{w}_s – any physics producing the same drift will produce the same linear instabilities.

We now Fourier decompose each variable, $\delta \propto \exp[i(\mathbf{k} \cdot \mathbf{x} - \omega t)]$, and define the parallel and perpendicular components of $\mathbf{k} \equiv k_{\parallel} \hat{\mathbf{w}}_s + k_{\perp} \hat{\mathbf{k}}_{\perp}$. Because of the symmetry of the problem, the solutions are independent of the orientation of $\hat{\mathbf{k}}_{\perp}$ in the plane perpendicular to $\hat{\mathbf{w}}_s$. The density equations trivially evaluate to $\delta\rho = \rho_0 \omega^{-1} \mathbf{k} \cdot \delta\mathbf{u}$ and $\delta\rho_d = \mu \rho_0 (\omega - \mathbf{w}_s \cdot \mathbf{k})^{-1} \mathbf{k} \cdot \delta\mathbf{v}$, and the momentum equations can be written

$$\begin{aligned} \omega \delta\mathbf{u} + (\omega - \mathbf{w}_s \cdot \mathbf{k}) \delta\mathbf{v} &= \frac{(c_s^2 \langle t_s \rangle \mathbf{k} - i\mu \mathbf{w}_s) \mathbf{k} \cdot \delta\mathbf{u}}{\omega \langle t_s \rangle} + \frac{(i\mu \mathbf{w}_s) \mathbf{k} \cdot \delta\mathbf{v}}{(\omega - \mathbf{w}_s \cdot \mathbf{k}) \langle t_s \rangle}, \\ i \mathbf{w}_s \frac{\delta t_s}{\langle t_s \rangle} &= \langle t_s \rangle (\omega - \mathbf{w}_s \cdot \mathbf{k}) \delta\mathbf{v} + i(\delta\mathbf{v} - \delta\mathbf{u}). \end{aligned} \quad (4)$$

In this form, the first equation is the total momentum equation for the sum gas+dust mixture. The next equation encodes our ignorance about t_s . To make further progress, we require a functional form for t_s to determine δt_s . For most physically interesting drag laws, t_s depends on some combination of the density, temperature, and velocity offset $|\mathbf{v} - \mathbf{u}|$ (more below). Therefore, for now, we consider an *arbitrary* t_s of the form $t_s = t_s(\rho, T, c_s, \mathbf{v} - \mathbf{u})$. Assuming there is some equation-of-state which can relate perturbations in T and c_s to ρ , then the linearized form obeys,

$$\frac{\delta t_s}{\langle t_s \rangle} = -\eta \frac{\delta\rho}{\rho_0} - \zeta \frac{\mathbf{w}_s \cdot (\delta\mathbf{v} - \delta\mathbf{u})}{|\mathbf{w}_s|^2}, \quad (5)$$

where η and ζ are the drag coefficients that depend on the form of t_s (see § 4).

2.2 Gas Supported By Pressure Gradients

Above we considered a freely accelerating frame. Another physically relevant case is when the gas is stationary and supported by a pressure gradient. We will include this possibility in our derivations below (§ 3), finding that it does not fundamentally change the character of the instability. The equilibrium solution has $\langle \mathbf{u} \rangle = \mathbf{0}$ and $\langle \nabla P \rangle = \langle \rho \rangle \mathbf{g} + \langle \rho_d \rangle \langle \mathbf{v} \rangle / \langle t_s \rangle$. If we consider length scales much shorter than the pressure-gradient scale-length $P/|\nabla P| \sim c_s^2 / |\mathbf{g} + \mu(\mathbf{g} + \mathbf{a})| \gg |\mathbf{k}|^{-1}$, then we usually expect the correction from ∇P is negligible. But because we will consider cases with, say, arbitrarily small μ , we wish to confirm this intuition explicitly.

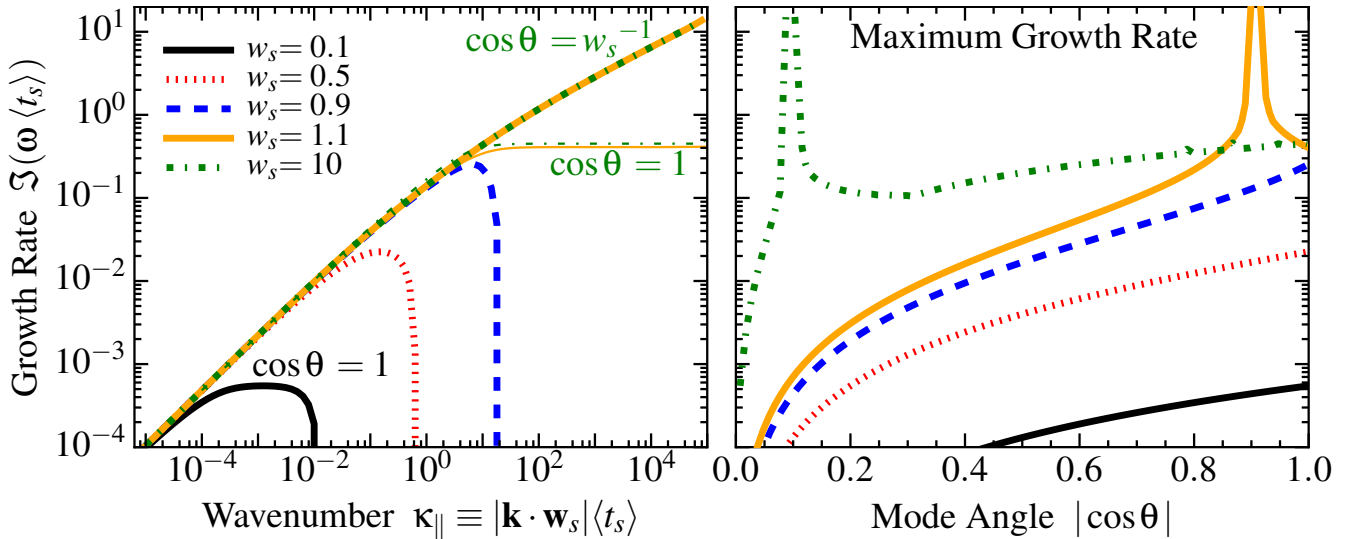


Figure 1. Linear growth rates of the acoustic RDI. We show the growth rate $\mathfrak{S}(\omega)$ of the fastest-growing unstable mode (in units of the equilibrium dust drag timescale or “stopping time” $\langle t_s \rangle$; Eq. (1)), for dust moving through gas with drift/streaming velocity $\mathbf{w}_s = w_s c_s \hat{\mathbf{w}}_s$ (Eq. (2); c_s is the gas sound speed), for different w_s (§ 2). Here we assume a mean dust-to-gas mass ratio $\mu = 0.1$ (Eq. (2)), constant drag coefficient ($\eta = \zeta = 0$; Eq. (5)), and a homogeneous background ($\phi = 0$; § 2.2). *Left:* Growth rate vs. wavenumber \mathbf{k} (§ 3), in terms of the dimensionless $\kappa_{\parallel} \equiv \mathbf{k} \cdot \mathbf{w}_s \langle t_s \rangle = k w_s c_s \langle t_s \rangle \cos \theta$ (Eq. (9)), and angle $\cos \theta \equiv \hat{\mathbf{k}} \cdot \hat{\mathbf{w}}_s$ between the wavevector \mathbf{k} and \mathbf{w}_s . For “subsonic” cases with $w_s < 1$, modes are unstable at long wavelengths (see § 3.4) with growth rates $\propto \kappa_{\parallel}^{2/3}$ (Eq. (10)) then saturate at a maximum growth rate, and are stabilized at high- k (§ 3.8). We show the fastest-growing angle $\cos \theta = 1$ for $w_s < 1$. Note that up to their saturation value, the different- w_s cases behave identically. For “supersonic cases” with $w_s \geq 1$, all k are unstable; at most angles the growth rate saturates at a constant value (the “intermediate” mode in § 3.6), but for $\cos \theta = \pm 1/w_s$ the “resonant” RDI appears (§ 3.7.1), where the drift velocity in the direction $\hat{\mathbf{k}}$ is resonant with the natural response frequency of the system (a sound wave), and the growth rates increase without limit as $\propto \kappa_{\parallel}^{1/2}$ (Eq. (16)) and $\propto \kappa_{\parallel}^{1/3}$ (Eq. (17)) at intermediate and high κ_{\parallel} , respectively. *Right:* Maximum growth rate (over all k) as a function of angle. For $w_s < 1$ this is maximized at finite growth rate, at $\cos \theta = \pm 1$; for $w_s \geq 1$, the maximum growth rates diverge around the “resonant angle.”

If we wish to retain the correction, then if ∇P is the result of a temperature gradient at constant density, the homogeneous solution is: $\rho^h = \rho_0$, $\rho_d^h = \mu \rho_0$, $\mathbf{u}^h = \mathbf{0}$, $\mathbf{v}^h = \mathbf{u}^h + \mathbf{w}_s$, with $\mathbf{w}_s = (\mathbf{g} + \mathbf{a}) \langle t_s \rangle$ and $P^h = P_0 + \rho_0 [\mathbf{g} + \mu (\mathbf{g} + \mathbf{a})] \cdot (\mathbf{x} - \mathbf{x}_0)$. Since \mathbf{x}_0 is arbitrary, linearize about $\mathbf{x} = \mathbf{x}_0$ and define $c_s^2 = (\partial P / \partial \rho)|_{\mathbf{x}=\mathbf{x}_0} \equiv \gamma P_0 / \rho_0$. The linearized equations are then identical to Eq. (3), with one addition:

$$\begin{aligned} \nabla \delta \rho &\rightarrow \nabla \delta \rho + \frac{\phi}{c_s \langle t_s \rangle} \delta \rho \\ \phi &\equiv \frac{(\gamma - 1)}{c_s} (\langle t_s \rangle \mathbf{g} + \mu \mathbf{w}_s) \end{aligned} \quad (6)$$

This is straightforward to include, and we will show it does not change the character of the solutions. However this addition requires two caveats: (1) obviously this solution *cannot* be valid over scales larger than the gradient scale-length $\sim c_s \langle t_s \rangle / \phi$, or else the pressure would be negative. We must therefore restrict to $k c_s \langle t_s \rangle \gg \phi$. And (2) even at high- k , an iso-density atmosphere with constant \mathbf{g} is convectively unstable with Brunt-Väisälä frequency $\sim i g / c_s$. Therefore we should consider this case heuristic unless we restrict to $\mathbf{g} = \mathbf{0}$ (where the pressure gradient only offsets acceleration from dust drag), but it is still illustrative.

For stratified atmospheres with $\rho = \rho(z)$, finding equilibrium solutions with steady-state drift and $\mathbf{u} = \mathbf{0}$ is difficult: what tends to happen is the dust has a quasi-steady-state drift where our “free streaming” approximation is valid for some time, but eventually the dust settles or is removed from the atmosphere. In those cases our derivation should be locally valid.

Finally, we note that because we restrict \mathbf{g} and $\hat{\mathbf{w}}_s$ to be parallel in the derivation above (such that the pressure gradient can support against the dust drag), the “Brunt-Väisälä RDI” – which results

from a resonance between dust and Brunt-Väisälä oscillations – is stable (see SH).

2.3 Neglected physics

2.3.1 Magnetized Gas and Dust

In this paper, we focus for simplicity on a pure hydrodynamic fluid. If the system is sufficiently magnetized, new wave families appear (e.g. shear Alfvén, slow, and fast magnetosonic waves in MHD). SH show that slow and fast magnetosonic waves, just like the acoustic waves here, are subject to the RDI (even when there is no Lorentz force on the dust). For resonant modes, when the projected dust streaming velocity ($\mathbf{w}_s \cdot \hat{\mathbf{k}}$) matches either the slow or fast wave phase velocity, the qualitative behavior is similar to the acoustic RDI studied here (§ 3.7.1). Further, like for hydrodynamic modes studied in detail below (§ 3), even modes that are not resonant can still be unstable (but, unsurprisingly, the MHD-dust system is more complicated; see Tytarenko et al. 2002). For these reasons, we defer a more detailed study of MHD to future work.

Another effect, which was not included in SH, is grain charge. If the gas is magnetized and the grains are sufficiently charged, then Lorentz forces may dominate over the aerodynamic drag laws we consider here. This regime is relevant to many astrophysical systems (even, e.g., cosmic ray instabilities; Kulsrud & Pearce 1969; Bell 2004). However, because the “grains” can no longer be treated as a pressureless fluid (particles undergo nontrivial drifts if the accelerating force is not parallel to the magnetic field), the physics of this regime is different and we leave its study to future work.

2.3.2 Multi-Species Dust

Astrophysical dust is distributed over a broad spectrum of sizes (and other internal properties), producing different t_s , \mathbf{v} , \mathbf{a} for dif-

ferent species. Consider de-composing the dust into sub-species i . Since the dust is pressure free, the dust continuity and momentum equations in Eq. (1) simply become a pair of equations for each sub-species i . Each has a continuity equation for $\rho_{d,i}$ (where $\rho_d = \sum_i \rho_{d,i}$) and momentum equation for \mathbf{v}_i , each with their own acceleration \mathbf{a}_i and drag $t_{s,i}$, but otherwise identical form to Eq. (1). The gas continuity equation is identical, and the gas momentum equation is modified by the replacement of the drag term $\rho_d (\mathbf{v} - \mathbf{u})/t_s \rightarrow \sum_i \rho_{d,i} (\mathbf{v}_i - \mathbf{u})/t_{s,i}$. The homogeneous solution now features each grain species moving with $\mathbf{w}_{s,i}$ where $\mathbf{w}_{s,i} \propto \mathbf{a}_i t_{s,i}$, so the sum in the gas momentum equation becomes $\sum_i \rho_{d,i} (\mathbf{v}_i - \mathbf{u})/t_{s,i} \sim \sum_i \mu_i \mathbf{a}_i$.

The most important grain property is usually size (this, to leading order, determines other properties such as charge). For a canonical spectrum of individual dust grain sizes (R_d), the total dust mass contained in a logarithmic interval of size scales as $\mu_i \propto d\mu/d \ln R_d \propto R_d^{0.5}$, i.e. most of the dust mass is concentrated in the largest grains (Mathis et al. 1977; Draine 2003). Further, for any physical dust law (see § 4), $t_{s,i}$ increases with R_d . In most situations, we expect $|\mathbf{a}_i|$ to depend only weakly on R_d . This occurs: (i) if the difference in dust-gas acceleration is sourced by gravity or pressure support for the gas, (ii) when the gas is directly accelerated by some additional force (e.g. radiative line-driving), or (iii) when the dust is radiatively accelerated by long-wavelength radiation.¹ Therefore, in these cases, all of the relevant terms in the problem are dominated by the largest grains, which contain most of the mass. We therefore think of the derivation here as applying to “large grains.” The finite width of the grain size distribution is expected to broaden the resonances discussed below (since there not exactly one $w_{s,i}$, there will be a range of angles for resonance), but not significantly change the dynamics. Much smaller grains can effectively be considered tightly-coupled to the gas (they will simply increase the average weight of the gas).

However, in some special circumstances – for example acceleration of grains by high-frequency radiation – we may have $|\mathbf{a}_i| \propto R_d^{-1}$. In these cases, the “back reaction” term on the gas is dominated by small grains, however those also have the smallest $w_{s,i}$ and $t_{s,i}$, and will thus have slower instability growth rates. There will therefore be some competition between effects at different grain sizes, and the different sizes may influence one another via their effects on the gas. This will be explored in future numerical simulations.

2.3.3 Viscosity

We neglect dissipative processes in the gas in Eqs. (3)–(4) (e.g., bulk viscosity). Clearly, including this physics will create a minimum scale below which RDI modes are damped. This is discussed more in § 6.

3 UNSTABLE MODES: GENERAL CASE

In this section, we outline, in full detail, the behavior of the dispersion relation that results from Eq. (4). While the completely

¹ If dust is radiatively accelerated by a total incident flux \mathbf{F}_λ centered on some wavelength λ , the acceleration is $\mathbf{a} \approx \mathbf{F}_\lambda Q_\lambda \pi R_d^2 / (cm_d) \propto Q_\lambda / R_d$, where $m_d \propto \bar{\rho}_d R_d^3$ is the grain mass and Q_λ is the absorption efficiency which scales as $Q_\lambda \sim 1$ for $\lambda \ll R_d$ and $Q_\lambda \sim R_d / \lambda$ for $\lambda \gg R_d$. So the acceleration scales $\propto 1/R_d$ for $\lambda \ll R_d$ and is independent of grain size for $\lambda \gg R_d$. For ISM dust, the typical sizes of the largest grains are $\sim 0.1 \mu\text{m} \sim 1000 \text{ \AA}$, so for most sources we expect to be in the long-wavelength limit (even in rare cases where sources peak at $\ll 1000 \text{ \AA}$, then gas, not dust, will typically be the dominant opacity source).

general case must be solved numerically, we can derive analytic expressions that highlight key scalings for all interesting physical regimes. To guide the reader, we start with a general overview of the different branches of the dispersion relation in § 3.1, referring to the relevant subsections for detailed derivations. For those readers most interested in a basic picture of the instability, Figs. 1–4 give a simple overview of the dispersion relation and its fastest-growing modes.

3.1 Overview of results

In general, the coupled gas-dust dispersion relation (Eq. (8) below) admits at least two unstable modes, sometimes more. This leads to a plethora of different scalings, each valid in different regimes, which we study in detail throughout § 3.2–3.9. The purpose of this section is then to provide a “road map” to help the reader to navigate the discussion.

An important concept, discussed above and in SH, is a mode “resonance.” This occurs when $\mathbf{w}_s \cdot \hat{\mathbf{k}} = c_s$, and thus is always possible (for some $\hat{\mathbf{k}}$) when $|\mathbf{w}_s| > c_s$ ($w_s > 1$). As shown in SH, when $\mu \ll 1$ (and $k \gg \mu$), modes at the resonant angle are the fastest growing, and will thus be the most important for dynamics. In the context of the analysis presented below, we will see that the dispersion relation changes character at resonance, and we must thus analyze these specific mode angles separately. The connection to the matrix-based analysis of SH, which treated only the resonant modes, is outlined in App. A. A clear illustration of the importance of the resonant angle is shown in the right-hand panel of Fig. 1.

Below, we separate our discussion into the following modes (i.e., regimes/branches of the dispersion relation):

(i) Decoupling instability, § 3.3: If $\zeta < -1$, the drag on the dust decreases with increasing w_s sufficiently fast that the dust and the dust completely decouple, causing an instability which separates the two. This instability exists for all \mathbf{k} , but is not usually physically relevant (see § 4.4).

(ii) Long-wavelength modes, § 3.4: At long wavelengths, the two unstable branches of the dispersion relation merge. This instability, which has a growth rate that scales as $\Im(\omega) \sim k^{2/3}$, persists for all μ , any w_s , and any η and ζ (except $\zeta = 0, \eta = 1$). A resonance does not modify the dispersion relation in this regime.

(iii) The “intermediate” mode, § 3.6: At shorter wavelengths, the two branches of the dispersion relation split in two. We term the first of these the “intermediate” mode. When $w_s \gtrsim c_s$, the intermediate mode is unstable for all k , with $\Im(\omega) \sim k^0$ (i.e., the growth rate is constant). At resonance (§ 3.6.1), the intermediate mode is subdominant and its growth rate declines with increasing k . The intermediate mode is stable for subsonic streaming ($w_s < 1$).

(iv) The “slow” mode, § 3.7: The second shorter-wavelength branch is the “slow” mode. At the resonant mode angle (§ 3.7.1), the slow mode is the dominant mode in the system, with a growth rate that increases without bound as $k \rightarrow \infty$. For a mid range of wavelengths $\Im(\omega) \sim k^{1/2}$, while for sufficiently short wavelengths $\Im(\omega) \sim k^{1/3}$. Away from resonance (e.g., if $w_s < 1$), the slow mode is either stable or its growth rate saturates at a constant value (i.e., $\Im(\omega) \sim k^0$), depending on w_s and $\eta/(1+\zeta)$.

(v) The “uninteresting” mode: For certain parameter choices a third unstable mode appears (it would be a fourth unstable mode if $\zeta < -1$, when the decoupling instability also exists). We do not analyze this mode further because it always has a (significantly) lower growth rate than either the intermediate or slow modes.

We also discuss the subsonic limit $w_s < 1$ separately in more detail (§ 3.8), so as to highlight key scalings for this important physical

regime. Finally, in § 3.9, we consider the structure of the eigenmodes for the fastest-growing modes (the long-wavelength mode and the resonant version of the slow mode), emphasizing how the resonant modes directly seed large dust-to-gas-ratio fluctuations in the gas.

3.2 General dispersion relation

Before continuing, let us define the problem. For brevity of notation, we will work in units of ρ_0 , c_s , and $\langle t_s \rangle$ (i.e. length units $c_s \langle t_s \rangle$), viz.,

$$w_s \equiv \frac{|\mathbf{w}_s|}{c_s}, \quad \omega \rightarrow \omega \langle t_s \rangle, \quad k \rightarrow k c_s \langle t_s \rangle. \quad (7)$$

Inserting the general form for t_s (Eq. (5)) into Eq. (4) (including pressure-gradient terms), we obtain the dispersion relation

$$0 = A_\omega B_\omega \quad (8)$$

$$A_\omega \equiv \mu + (\omega + i\mu)(\omega' + i)$$

$$B_\omega \equiv i w_s^2 \mu \left[w_s^2 \mu \left(\omega^3 \tilde{\zeta} - \omega^2 \kappa_{\parallel} (2\tilde{\zeta} + \eta - 1) + \omega \kappa_{\parallel}^2 (2\eta + \tilde{\zeta} - 2) \right. \right. \\ \left. \left. + \kappa_{\parallel}^2 \{ \kappa_{\parallel} (1 - \eta) - i(\tilde{\zeta} - \eta) \} \right) - i(\omega' + i\tilde{\zeta}) \left(\omega^3 w_s^2 \right. \right. \\ \left. \left. - \omega^2 \kappa_{\parallel} w_s^2 - \omega \kappa_{\parallel} (\kappa_{\parallel} - i w_s \phi) + \kappa_{\parallel} (w_s^2 k^2 - i \kappa_{\parallel} w_s \phi) \right) \right] \\ - w_s^2 (\omega' + i) \left[(w_s^2 k^2 - \kappa_{\parallel}^2) (i \mu \tilde{\zeta} (\omega'^2 - i \kappa_{\parallel}) + \omega \omega' (\omega' + i \tilde{\zeta})) \right. \\ \left. + (\mu - i\omega) \left(w_s^2 \mu \{ \omega^3 \tilde{\zeta} - \omega^2 \kappa_{\parallel} (2\tilde{\zeta} + \eta - 1) \right. \right. \right. \\ \left. \left. + \omega \kappa_{\parallel}^2 (\tilde{\zeta} + 2\eta - 2) + \kappa_{\parallel}^2 [\kappa_{\parallel} (1 - \eta) - i(\tilde{\zeta} - \eta)] \} \right) \right. \\ \left. - i \omega' (\omega' + i \tilde{\zeta}) (w_s^2 w_s^2 - \kappa_{\parallel}^2 + i \kappa_{\parallel} w_s \phi) \right]$$

where

$$\omega' \equiv \omega - \kappa_{\parallel}, \quad \tilde{\zeta} \equiv 1 + \zeta \\ \kappa_{\parallel} \equiv \mathbf{k} \cdot \mathbf{w}_s = k_{\parallel} w_s = w_s k \cos \theta. \quad (9)$$

(Note that $\cos \theta$, the angle between $\hat{\mathbf{k}}$ and $\hat{\mathbf{w}}_s$, was denoted ψ_{kw} in SH to allow for simpler notation in the MHD case.)

Our task is to analyze the solutions to Eq. (8). Fig. 1 plots the growth rate of the fastest-growing modes at each κ_{\parallel} for a range of w_s , determined by exact numerical solution of Eq. (8). Figs. 2, 3, and 4 show additional examples.

3.2.1 General considerations

In Eq. (8), A_ω has the uninteresting zeros $2\omega = \kappa_{\parallel} - i(1 + \mu) \pm [\kappa_{\parallel}^2 - (1 + \mu)^2 - i2\kappa_{\parallel}(1 - \mu)]^{1/2}$. These are damped longitudinal sound waves which decay ($\Im(\omega) \leq 0$) on a timescale $\sim \langle t_s \rangle$ for all μ and κ_{\parallel} ; they are independent of η and ζ . The interesting solutions therefore satisfy $B_\omega = 0$, a sixth-order polynomial in ω .

For fully-perpendicular modes ($\mathbf{k} = \mathbf{k}_{\perp}$), $B_\omega = 0$ simplifies to $\omega^2 (\omega + i\tilde{\zeta}[1 + \mu]) [\omega^2 (i[1 + \mu] + \omega) - k^2 (i + \omega)] = 0$; this has the solutions $\omega = 0$, $\omega = -i(1 + \mu)\tilde{\zeta}$, and the solutions to $\omega^2 (i[1 + \mu] + \omega) - k^2 (i + \omega) = 0$ which correspond to damped perpendicular sound waves and decay ($\Im(\omega) < 0$) for all physical $\mu > 0$. For the general physical situation, with $\tilde{\zeta} > 0$, all unstable modes must thus have $k_{\parallel} \neq 0$.

3.3 Decoupling Instability

Before considering the more general case with $k_{\parallel} \neq 0$, it is worth noting that the perpendicular ($k_{\parallel} = 0$) mode above, $\omega = -i(1 + \mu)\tilde{\zeta}$ is unstable if $\tilde{\zeta} < 0$, i.e. $\zeta < -1$. Physically, this is the statement that the dust-gas coupling becomes weaker at higher relative velocities, and instability can occur when dust and gas de-couple

from one another (the gas decelerates and returns to its equilibrium without dust coupling, while the dust moves faster and faster as it accelerates, further increasing their velocity separation). As discussed below (Sec. 4.4) this could occur for Coulomb drag with $w_s \gg 1$; however, in this regime Coulomb drag will never realistically dominate over Epstein or Stokes drag, so we do not expect this instability to be physically relevant.

3.4 Long-Wavelength Instability: $\kappa_{\parallel} \ll \hat{\mu}$

We now examine the case of long wavelengths (small k) in the free-accelerating case ($\phi = 0$). If we consider terms in ω up to $\mathcal{O}(k)$ for $k \ll 1$, and expand B_ω , we obtain $\omega^3 \tilde{\zeta} (1 + \mu) = i\mu (\tilde{\zeta} - \eta) \kappa_{\parallel}^2$ to leading order. For $\tilde{\zeta} - \eta > 0$, this has two unstable roots with the same imaginary part but oppositely-signed real parts (waves propagating in opposite directions are degenerate). Solving B_ω up to $\mathcal{O}(k)$ gives:

$$\omega(\kappa_{\parallel} \ll \hat{\mu}) \approx \begin{cases} \kappa_0 + \frac{\pm\sqrt{3} + i}{2} \left(1 - \frac{\eta}{\tilde{\zeta}}\right)^{\frac{1}{3}} \hat{\mu}^{1/3} \kappa_{\parallel}^{2/3} & (\eta < \tilde{\zeta}) \\ \kappa_0 + i \left(\frac{\eta}{\tilde{\zeta}} - 1\right)^{\frac{1}{3}} \hat{\mu}^{1/3} \kappa_{\parallel}^{2/3} & (\eta > \tilde{\zeta}) \end{cases} \quad (10)$$

$$\kappa_0 \equiv \left[1 + \mu \left(2 + \frac{\eta - 1}{\tilde{\zeta}}\right)\right] \frac{\kappa_{\parallel}}{3(1 + \mu)}, \quad \hat{\mu} \equiv \frac{\mu}{1 + \mu}$$

Note that this mode depends only on $\kappa_{\parallel} = w_s k \cos \theta$ at this order; the dependence on w_s is implicit. The growth rate rises towards shorter wavelengths, but sub-linearly. Most notably, instability exists at *all* dust abundances μ (and depends only weakly on that abundance, with the $1/3$ power), wavelengths κ_{\parallel} (for $\kappa_{\parallel} \ll \hat{\mu}$), accelerations w_s , and drag coefficients η and ζ .²

If instead of the free-accelerating frame, we consider the pressure-supported case with sufficiently large $|\phi|$, then series expansion at small k gives, to leading-order, $\omega^2 w_s (1 + \mu) = -i\phi k$. This has the growing solution $\omega \approx (\pm 1 + i) \{|\phi| k / [2(1 + \mu)]\}^{1/2}$. When $\mathbf{g} = 0$ (i.e. $\phi = (\gamma - 1)\mu w_s$), this is similar to the mode above. For large \mathbf{g} (see Eq. (6)), the frequency in physical units is $\omega \sim i\sqrt{gk}$, which is the normal gas convective instability, as expected (see § 2.2). As noted in § 2.2 these modified solutions where ϕ dominates apply only in the limit where the wavelength is larger than the pressure scale-height, so they are somewhat pathological.

3.5 Short(er)-Wavelength Instabilities: $\kappa_{\parallel} \gg \hat{\mu}$

At high- k there are at least two different unstable solutions. If we assume a dispersion relation of the form $\omega \sim \mathcal{O}(k^1) + \mathcal{O}(k^\nu)$ where $\nu < 1$, and expand B_ω to leading order in $k^{-1} \ll 1$, we obtain a dispersion relation $0 = \omega(\omega - \kappa_{\parallel})^3 (\omega^2 - k^2) (1 + \mathcal{O}(k^{-1}))$. This is solved by $\omega = \pm k + \mathcal{O}(k^\nu)$ or $\omega = \kappa_{\parallel} + \mathcal{O}(k^\nu)$, each of which produces a high- k branch of the dispersion relation.

In the following sections, 3.6–3.7, we study each of these branches in detail. We term the first branch, with $\omega = \pm k + \mathcal{O}(k^\nu)$, the “intermediate” mode (§ 3.6); we term the second branch, with $\omega = \kappa_{\parallel} + \mathcal{O}(k^\nu)$, the “slow” mode (§ 3.7). In the analysis of each of

² Note that in the pathological case $\eta = \tilde{\zeta} = 1 + \zeta$, our approximation in Eq. (10) vanishes but an exact solution to Eq. (8) still exhibits low- k instability, albeit with reduced growth rate. The reason is that the leading-order term on which Eq. (10) is based vanishes, so the growth rate scales with a higher power of κ_{\parallel} . Instability only vanishes completely at low- k when $\eta = 1$ and $\zeta = 0$, exactly.

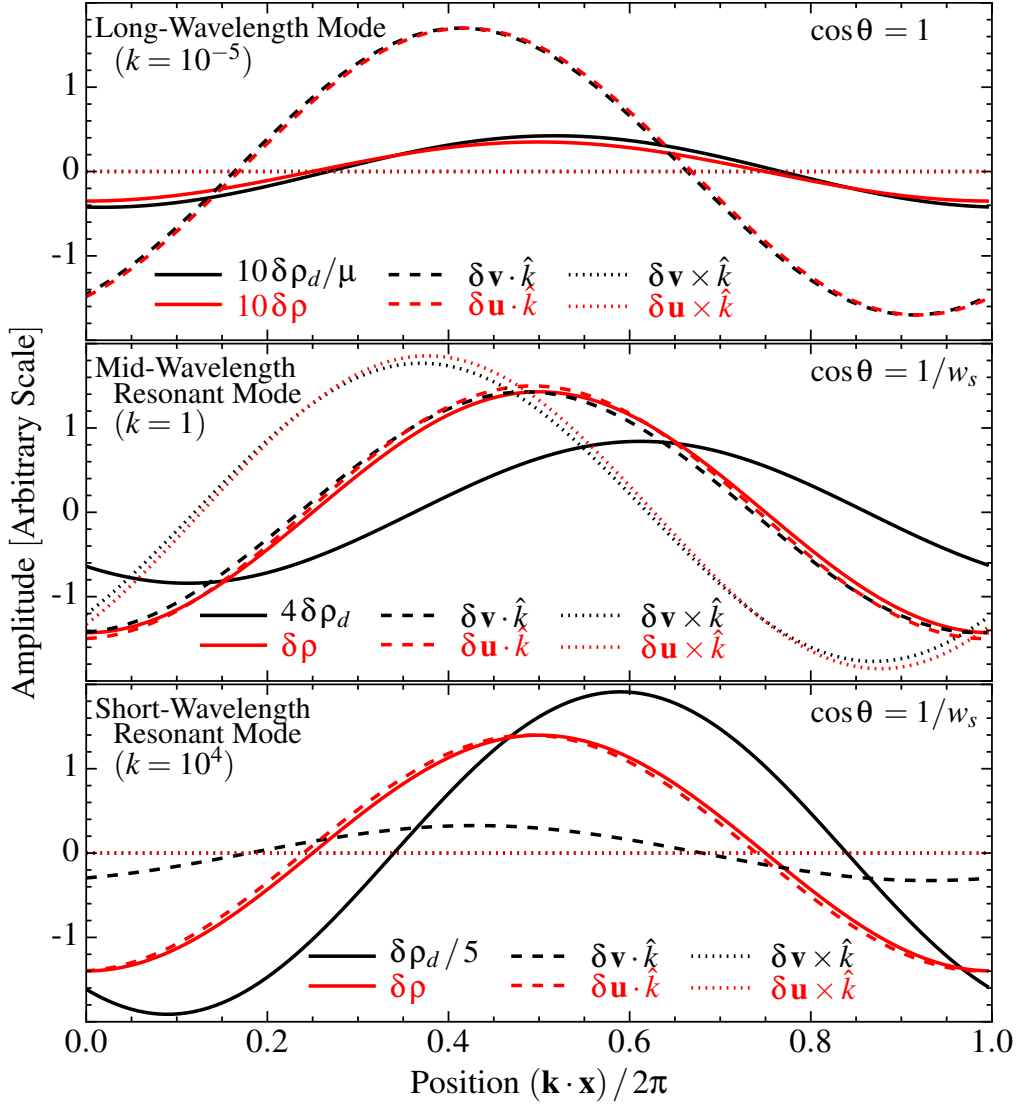


Figure 2. Spatial structure of the modes in Fig. 1 (see § 3.9). Here we take $\mu = 0.01$, $\eta = \zeta = \phi = 0$, $w_s = 10$, and $\cos\theta$ shown, and plot the perturbed dust density $\delta\rho_d$, gas density $\delta\rho$ (in units of ρ_0 , the mean density) and perturbed dust velocity $\delta\mathbf{v}$ and gas velocity $\delta\mathbf{u}$ (in units of c_s). The overall amplitude of the linear perturbation (y-axis normalization) is arbitrary. For the velocities we separate them into the magnitude of the component parallel to $\hat{\mathbf{k}}$ ($\delta\mathbf{v} \cdot \hat{\mathbf{k}}$), and perpendicular ($\delta\mathbf{v} \times \hat{\mathbf{k}}$). We show the spatial structure over one period, for a given k (in units of $c_s \langle t_s \rangle$). In all cases, a lag between the dust and gas density perturbations arises because the dust de-accelerates when moving through the denser gas, which generates a “pileup” and stronger dust-density peak, which in turn amplifies the gas response. *Top:* The long-wavelength mode exhibits a nearly-coherent dust-gas oscillation, with $\delta\rho_d \approx \mu \delta\rho$ to leading order (the lag is higher-order). This is not a modified sound wave, however: the phase/group velocities scale $\propto k^{-1/3}$, the velocity and density responses are offset by a phase lag, and the gas+dust density perturbation is weak ($|\delta\rho|/\rho_0 \ll |\delta\mathbf{v}|/c_s$; note we multiply $\delta\rho$ plotted by 10, and $\delta\rho_d$ by $10/\mu$). *Middle:* Resonant mode, at intermediate wavelengths where the growth rate scales $\propto k^{1/2}$. The wavespeed, gas density and velocity in the $\hat{\mathbf{k}}$ direction now behave like a sound wave. The dust lag is larger (phase angle $\sim \pi/6$) and because of the “resonance,” where the dust motion along the $\hat{\mathbf{k}}$ direction exactly matches the wavespeed, the effects above add coherently and generate a much stronger dust response with $|\delta\rho_d|/|\delta\rho| \sim (2\mu k)^{1/2}$, a factor $\sim (2k/\mu)^{1/2} \sim 20$ larger than the mean dust-to-gas ratio. Note the large perpendicular velocities also present. *Bottom:* Resonant mode, at short wavelengths (where the growth rate scales $\propto k^{1/3}$). This is similar to the intermediate-wavelength case except the perpendicular velocities become negligible, the dust velocity response $\delta\mathbf{v}$ becomes weaker, but the dust density response continues to become stronger, with $|\delta\rho_d|/|\delta\rho| \sim (4\mu k)^{1/3}$, a factor ~ 1000 larger here than the mean dust-to-gas ratio μ .

these, we must treat modes with the resonant angle, $\cos\theta = \pm 1/w_s$, separately, because the dispersion relation fundamentally changes character. The intermediate mode at resonance (§ 3.6.1) is modified only in minor ways. In contrast, the slow mode at resonance (§ 3.7.1) is the fastest-growing mode in the system (when $w_s > 1$ and $\mu \ll 1$), with growth rates that increase *without bound* as $k \rightarrow \infty$. This is the acoustic RDI studied in SH (see also App. A).

3.6 Short(er)-Wavelength Instability: The “Intermediate” Mode

To leading-order, the intermediate mode satisfies $\omega = \pm k$. Consider the next-leading-order term; i.e. assume $\omega = \omega_{\text{med}} = \pm k + \varpi + \mathcal{O}(k^{-1})$ (where ϖ is a term that is independent of k) and expand the dispersion relation to leading order in k^{-1} (it will transpire that the solution here is valid for all $k \gg w_s \mu$). This produces a simple

linear leading-order dispersion relation for both the \pm cases:

$$\omega_{\text{med}} \approx \pm k - i \frac{\mu(1 + \zeta \cos^2 \theta \pm w_s(1 - \eta) \cos \theta) \pm \phi \cos \theta}{2} \quad (11)$$

Where the “+” mode applies the + to all \pm , and vice versa.

First consider the free-accelerating ($\phi = 0$) case. Because both signs of $\cos \theta$ are allowed, it follows that the modes are unstable ($\Im(\omega) > 0$) if

$$w_s |(1 - \eta) \cos \theta| > 1 + \zeta \cos^2 \theta. \quad (12)$$

Because ζ and η generally are order-unity or smaller, Eq. (12) implies that $w_s \gtrsim 1$ is required for this mode to be unstable. For $\zeta < 1$, the more common physical case (see § 4), we also see that the condition (12) is first met for parallel modes ($\cos \theta = \pm 1$) and that their growth rate (11) is larger than oblique modes.³ Comparing the long-wavelength result (10) to Eq. (11), we see that the growth rate grows with k until it saturates at the constant value given by Eq. (11) above $k \gtrsim w_s \mu$. For $w_s \lesssim 1$, the mode becomes stable above $k \gtrsim w_s \mu$.

In the pressure-supported case, $\phi \neq 0$ can additionally destabilize the system and lead to large growth rates $\sim |\phi|/2$ (for either sign of ϕ , if $|\phi| \gg \mu w_s$), with the growth rate maximized for $\cos \theta = \pm 1$. This is just the convective instability of the gas.

3.6.1 The Intermediate Mode at Resonance

When $w_s \cos \theta = \pm 1$, the behavior of the intermediate mode is changed (the series expansion we used is no longer valid; see § 3.7.1): instead of the growth rate becoming constant at high- k , it peaks around $\kappa_{\parallel} \sim \hat{\mu}$ at a value $\Im(\omega) \approx \hat{\mu}/4$, and then declines with increasing κ_{\parallel} . It is therefore the less interesting mode in this limit.

3.7 Short(er) Wavelength Instability: The “Slow” Mode

We now consider the slow mode branch of the high- k limit of ω , with $\omega = \kappa_{\parallel} + \mathcal{O}(k^\nu)$. Assuming $\omega = \omega_{\text{slow}} = \kappa_{\parallel} + \varpi + \mathcal{O}(k^{-1})$, and expanding to leading order in k , we obtain the leading-order cubic relation

$$0 = \varpi(\varpi + i)(\varpi + i\tilde{\zeta})(1 - w_s^2 \cos^2 \theta) - \mu(i(\tilde{\zeta} - \eta)w_s^2 \cos^2 \theta + \varpi(1 - \tilde{\zeta} + (\tilde{\zeta}(1 + w_s^2) - w_s^2 \eta - 1) \cos^2 \theta)). \quad (13)$$

Note that at this order in the expansion in k , the ϕ terms from gas pressure gradients do not appear at all (they are suppressed relative to all terms here by $\mathcal{O}(k^{-1})$). The slow mode is thus identical in pressure-supported and free-accelerating systems.

Equation (13) is solvable in closed form but the expressions are tedious and unintuitive.⁴ For clarity of presentation, if we consider $\mu \ll 1$, the expression factors into a damped solution with

³ For the parallel case, the general dispersion relation B_ω simplifies to: $B_\omega \rightarrow A_\omega B'_\omega$ with

$$B'_\omega = \kappa_{\parallel} w_s^2 \mu (\omega \tilde{\zeta} - \kappa_{\parallel} \eta) + \omega' \left((\omega' + i\tilde{\zeta})(\omega^2 w_s^2 - \kappa_{\parallel}^2) + i w_s^2 \mu (\omega^2 \tilde{\zeta} + \kappa_{\parallel} \{ \kappa_{\parallel} (\eta - 1) + i\tilde{\zeta} \} - \omega \kappa_{\parallel} (\tilde{\zeta} + \eta - 1)) \right)$$

⁴ Eq. (13) does provide a simple closed-form solution if $\cos \theta = \pm 1$ (parallel modes), or $\zeta = 0$; in these cases the growing mode solutions are:

$$\omega_{\text{slow}}(|\cos \theta| = 1) \approx \kappa_{\parallel} + i \frac{\tilde{\zeta}}{2} \left[-1 + \left(1 + \frac{4\mu(\tilde{\zeta} - \eta)}{\tilde{\zeta}^2(1 - w_s^2)} \right)^{1/2} \right]$$

$$\omega_{\text{slow}}(\zeta = 0) \approx \kappa_{\parallel} + i \frac{1}{2} \left[-1 + \left(1 + \frac{4\mu(1 - \eta)}{1 - (w_s \cos \theta)^{-2}} \right)^{1/2} \right]$$

$\varpi = -i$, and a quadratic that gives a damped and a growing solution which simplifies to:

$$\omega_{\text{slow}}(\mu \ll 1) \approx \kappa_{\parallel} + i \frac{(w_s \cos \theta)^2 \mu}{(w_s \cos \theta)^2 - 1} \left(1 - \frac{\eta}{\tilde{\zeta}} \right) \quad (14)$$

This illustrates the general form of the full expression. In particular, we see that the expressions become invalid ($\Im(\omega) \rightarrow \infty$) at the resonant angle $w_s^2 \cos^2 \theta = 1$, which will be treated separately below (§ 3.7.1).

The requirement for instability (from the general version of Eq. (14)) is:

$$(w_s^2 \cos^2 \theta - 1)(1 - \eta/\tilde{\zeta}) \geq 0 \quad (15)$$

We thus see that if $\eta/\tilde{\zeta} < 1$ (the more common physical case), this mode is unstable for $w_s |\cos \theta| > 1$; if $\eta/\tilde{\zeta} > 1$, however, the mode is stable for $w_s |\cos \theta| > 1$ but becomes unstable for $w_s |\cos \theta| < 1$.

Away from resonance (i.e., with $|w_s \cos \theta| \neq 1$), we see that, like the intermediate mode, the slow mode is described by the long-wavelength solution from § 3.4, with a growth rate that increases with k until it saturates at the constant value of Eq. (14): roughly $\sim w_s^2 \mu$ for $w_s < 1$ or $\sim \mu$ for $w_s > 1$. Comparing the growth rates (Eq. (14) and Eq. (10)) we see this occurs at $k \gtrsim \mu w_s^2 / (1 + w_s^3)$ (i.e. $\sim w_s^2 \mu$ for $w_s < 1$, $\sim \mu/w_s$ for $w_s > 1$).

3.7.1 The Slow Mode at Resonance

When $w_s \geq 1$, then Eq. (14) (and its generalization, valid at all μ) diverge as $\cos \theta \rightarrow \pm 1/w_s$. In this case the “saturation” or maximum growth rate of the mode becomes infinite. What actually occurs is that the growth rate continues to increase *without limit* with increasing k .

In this limit, our previous series expansion at high- k is invalid: we must return to B_ω and insert $w_s \cos \theta = \pm 1$; i.e. $k^2 = \kappa_{\parallel}^2$ or $\mathbf{k} \cdot \mathbf{w}_s = \omega_{\text{sound}} \equiv \pm c_s k$, the resonance condition for the RDI. The resulting dispersion relation has growing solutions with $\Im(\omega_*) > 0$ for all κ_{\parallel} , and the growth rate increases monotonically with κ_{\parallel} without limit (here and below we use ω_* to denote the resonant frequency).⁵

If $\hat{\mu} \ll k \ll \hat{\mu}^{-1}$, the resonant solutions to $B_{\omega_*} = 0$ lead to the “mid- k ” resonant mode:

$$\omega_* (\hat{\mu} \ll \kappa_{\parallel} \ll \hat{\mu}^{-1}) \approx \kappa_1 + \frac{i \pm 1}{2} \left(\left| 1 - \frac{\eta}{\tilde{\zeta}} \right| \hat{\mu} \kappa_{\parallel} \right)^{1/2}$$

$$\kappa_1 \equiv \left[1 - \frac{\hat{\mu}}{4} \left(1 - \frac{\tilde{\zeta} \zeta + \eta w_s^2}{\tilde{\zeta}^2 w_s^2} \right) \right] \kappa_{\parallel} - i \frac{(\tilde{\zeta} - \eta) \hat{\mu}}{8 \tilde{\zeta}}. \quad (16)$$

As expected, to $\mathcal{O}(\mu^{1/2})$, this matches the “acoustic RDI” expression derived in SH, with a resonance between the dust drift velocity and an acoustic wave (the exact correspondence is explained in detail in App. A).

At larger $\kappa_{\parallel} \gg \hat{\mu}^{-1}$, expanding $\omega \sim \mathcal{O}(k)$ to leading order in $k \gg 1$ shows that the leading-order term must obey $\omega = \pm \kappa_{\parallel} = \pm k$, as before. Now expand to the next two orders in k as $\omega_* + k + \omega_{1/3} k^{1/3} + \varpi$, where again ϖ denotes a k -independent part (it is easy to verify that with $\nu \geq 0$, any term $\omega = k + \omega_\nu k^\nu$, other than $\nu = 0$ and $\nu = 1/3$, must have $\omega_\nu = 0$ to satisfy the dispersion relation to next-leading order in k). This gives $2\omega_{1/3}^3 + (1 + \zeta/w_s - \eta)\mu = 0$, and a simple linear expression for ϖ . There is always one purely real root, one decaying root, and one unstable $\Im(\omega) >$

⁵ Note that at long wavelengths, $k \ll \hat{\mu}$, the series expansion in Eq. (10) is still accurate and we just obtain the solutions in § 3.4, even at resonance.

0 root. Taking the unstable root, we obtain the “high- k ” resonant mode:

$$\omega_*(k \gg \hat{\mu}^{-1}) \approx \kappa_{\parallel} + (i\sqrt{3} \pm 1) \left(\frac{|\Theta| \mu \kappa_{\parallel}}{16} \right)^{1/3} - i\varpi \quad (17)$$

$$\Theta \equiv 1 + \frac{\zeta}{w_s^2} - \eta$$

$$\varpi \equiv \frac{(1+\Theta)\mu + \phi}{6} + \frac{1 + (\zeta^2 - 1)/w_s^2 - \zeta\eta}{3\Theta},$$

where the sign in the \pm part of the real part of ω_* is “+” if $\Theta > 0$ and “-” if $\Theta < 0$. Again this is just the high- k expression for the acoustic RDI derived in SH.

Qualitatively, the resonant modes grow in a similar way to the long-wavelength instability Eq. (10). We see that the slope decreases with increasing κ_{\parallel} from $\omega \sim \kappa_{\parallel}^{2/3}$ (for $\kappa_{\parallel} \ll \hat{\mu}$), to $\omega_* \sim \kappa_{\parallel}^{1/2}$ (for $\hat{\mu} \ll \kappa_{\parallel} \ll \hat{\mu}^{-1}$), to $\omega_* \sim \kappa_{\parallel}^{1/3}$ (for $\hat{\mu}^{-1} \ll \kappa_{\parallel}$). Comparison to the intermediate mode (Eq. (11)) or the slow mode away from resonance (Eq. (14)) shows that the resonant mode (Eqs. (16) and (17)) always grows fastest. Because resonance requires $w_s \cos \theta = \pm 1$, we have: $k_{\parallel} = k \cos \theta = \pm k/w_s$, $k_{\perp} = |\mathbf{k}_{\perp}| = k \sin \theta = k(1 - w_s^{-2})^{1/2}$, and $k_{\parallel}/k_{\perp} = \pm 1/\sqrt{w_s^2 - 1}$. For modest $w_s \gtrsim 1$, the resonant mode is primarily parallel ($\cos \theta \sim \pm 1$), but for large $w_s \gg 1$, the resonant mode becomes increasingly transverse, with $\theta \rightarrow \pi/2$ and $k_{\perp} \gg |k_{\parallel}|$.

Not surprisingly, since these modes are an extension of the out-of-resonance slow modes where the pressure support term ϕ did not appear, the term here only appears in the lowest-order ϖ term – it has no effect on the behavior, but just shifts the growth rate at a given k by a small constant.

At high- k and at resonance, anti-aligned solutions of the form $\omega = -k + \varpi + \mathcal{O}(k^{-1})$ are also admitted. These have the simple solution $\varpi \approx -i(\zeta + w_s \eta) \mu / (2w_s)$, which is growing only if $\zeta + w_s \eta < 0$.

3.8 Subsonic ($w_s < 1$) Modes

In § 3.7 above, we saw that when $w_s > 1$ (and $\hat{\mu} \ll 1$) the fastest growing modes will be the long-wavelength mode (at low k) and the acoustic RDI “resonant” modes (at high k). When the streaming is subsonic ($w_s < 1$) a resonance is no longer possible and the intermediate mode (§ 3.6) is also stabilized. It thus seems helpful to cover the subsonic mode structure in a self-contained manner, which is the purpose of this section. We collect some of the results derived in § 3.4–§ 3.7 and derive a new limit of the subsonic slow mode.

At low k , the long-wavelength solutions from § 3.4 continue to be unstable. Moreover, the “slow mode” in Eq. (14) is still unstable if $\eta > \zeta$ (see Eq. (15); in this case all k are unstable). The mode then grows as in Eq. (10) until saturating at a maximum growth rate given by Eq. (14): approximately $\sim w_s^2 \mu$, for $k \gtrsim w_s^2 \mu$. From the form of Eq. (14) we can also see that for $w_s < 1$ the most rapidly-growing mode has $\cos \theta = \pm 1$, i.e. the modes are parallel.

If $\zeta > \eta$ (and $w_s < 1$), the slow mode is stabilized for $k \gg 1$. However it persists for some intermediate range of k , which was not included in Eq. (14) due to our assumption $k \gg 1$. Specifically, the growth of $\Im(\omega)$ with κ_{\parallel} saturates at a similar point, but then $\Im(\omega)$ turns over and vanishes at finite $k \gtrsim w_s$. Since we are interested in small w_s and low- k , we assume $\omega \sim \varpi + \omega_1 w_s + \omega_2 w_s^2$ and $k \sim \mathcal{O}(w_s)$, and expand the dispersion relation to leading order in w_s . This gives two results: (i) that ϖ must vanish, and (ii) that ω_1 must obey $\omega_1(\omega_1^2(1+\mu) - (k/w_s)^2) = 0$. This gives the leading-order solution $\omega = \pm k_{\parallel} / \sqrt{1+\mu}$. Plugging in either the + or – root (they

give the same growth rate), we solve for the second-order term, to obtain the relation

$$\omega_{\text{subsonic}} \approx k_{\parallel} \left(\pm \frac{1}{(1+\mu)^{1/2}} + \frac{(\eta + \zeta w_s) w_s \mu}{2(1+\mu)\zeta} \right) + i \frac{\mu}{2} \left(w_s^2 (\zeta - \eta) - \frac{k_{\parallel}^2}{(1+\mu)^2} \right). \quad (18)$$

We see that this subsonic slow mode is unstable for $k_{\parallel} < w_s(1+\mu)(\zeta - \eta)^{1/2}$. We reiterate that Eq. (18) is valid only for $\zeta > \eta$; otherwise Eq. (14) is correct and all k are unstable.

3.9 Mode Structure

In this section we discuss the structure of the eigenmodes in $(\delta\rho, \delta\mathbf{u}, \delta\rho_d, \delta\mathbf{v})$. We focus on the most relevant (fastest-growing) modes in the three limits: (i) $\kappa_{\parallel} \ll \hat{\mu}$ (dispersion relation (10)), (ii) $\hat{\mu} \ll \kappa_{\parallel} \ll \hat{\mu}^{-1}$ (dispersion relation (16)), and (iii) $\kappa_{\parallel} \gg \hat{\mu}^{-1}$ (dispersion relation (17)). In the subsonic streaming limit $w_s < 1$, the long-wavelength mode is the most relevant. Examples of each are shown in Fig. 2.

(i) **Long-Wavelength Mode** ($\kappa_{\parallel} \ll \hat{\mu}$; Eq. (10)): As $k \rightarrow 0$, the fastest-growing mode has $\mathbf{k} \propto \mathbf{w}_s$ (i.e. $\cos \theta = \pm 1$), and the perturbed velocities are parallel: $\delta\mathbf{v} \propto \delta\mathbf{u} \propto \mathbf{k} \propto \mathbf{w}_s$. Moreover $\delta\mathbf{v} \approx \delta\mathbf{u}$ and $\delta\rho_d \approx \mu \delta\rho$. In other words the mode simply features *coherent* oscillations of the dust and gas together, because these modes have wavelengths larger than the deceleration length of the dust. To leading order, the mode does not generate fluctuations in the dust-to-gas ratio. A second order phase offset does appear between the dust and gas perturbations, and this drives the growth. But this offset is weak and the growth rate is correspondingly small.

However, the long-wavelength mode is not a perturbed sound wave (coupled dust-gas soundwaves exist at low- k , but these are damped). The phase and group velocities scale $\sim \mathbf{w}_s (k w_s / \mu)^{-1/3} \propto k^{-1/3}$, diverging as $k \rightarrow 0$ because of the leading-order term in $\omega \propto k^{2/3}$. There is also a phase offset, whereby the velocity perturbations lead (follow) the density perturbations by a phase angle of $\sim \pi/6$ for $w_s > 1$ ($w_s < 1$).⁶ This implies that the gas density response to the velocity perturbations is distinct from a sound wave, satisfying $\delta\rho/\rho_0 \sim w_s^{-1} (\kappa_{\parallel}/\mu)^{1/3} |\delta\mathbf{v}/c_s| \sim [k/(\mu w_s^2)]^{1/3} |\delta\mathbf{v}/c_s|$.

(ii) **Resonant Mode, Intermediate-Wavelengths** ($\hat{\mu} \ll \kappa_{\parallel} \ll \hat{\mu}^{-1}$; Eq. (16)): For intermediate k with $w_s \geq 1$, the fastest-growing mode has \mathbf{k} oriented at the resonant angle $\cos \theta = \pm 1/w_s$ (i.e. $\kappa_{\parallel} = k$, with $k_{\parallel} = \pm k/w_s$), so for $w_s \gg 1$ it is increasingly transverse ($k \approx k_{\perp}$). To leading order in k and μ , $\omega \approx c_s k$ so the wave phase/group velocity $= c_s \hat{\mathbf{k}}$. This is the key RDI resonance: the wavespeed matches that of the system without dust (in this case a sound wave), with a wavevector angle $\cos \theta = \pm 1/w_s$, such that the dust drift velocity in the direction of the wave propagation is equal to the wavespeed: $\mathbf{w}_s \cdot \hat{\mathbf{k}} = c_s$. In other words, the dust is co-moving with the wave in the direction $\hat{\mathbf{k}}$.

For $\mu \ll 1$, the gas density response behaves like a sound wave, $\delta\rho/\rho_0 \approx \hat{\mathbf{k}} \cdot \delta\mathbf{u}/c_s$, in-phase with the velocity in the $\hat{\mathbf{k}}$ -direction. However, the dust density response now lags by a phase angle $\sim \pi/6$, and, more importantly, the resonance generates a strong dust density response: $|\delta\rho_d| \sim (2\mu\kappa_{\parallel})^{1/2} |\delta\rho|$. We see the dust-density fluctuation is enhanced by a factor $\sim (2\kappa_{\parallel}/\mu)^{1/2} \gg 1$ relative to the mean (μ), which is much stronger than for the

⁶ The phase angle $\pi/6$ (the argument of $i^{1/3}$) appears repeatedly because the dominant imaginary terms in the dispersion relation are cubic.

long-wavelength mode (with $\delta\rho_d \sim \mu\delta\rho$). The resonant mode can thus generate very large dust-to-gas fluctuations even for otherwise weak modes, and the magnitude of the induced dust response increases at shorter wavelengths.

Effectively, as the dust moves into the gas density peak from the sound wave, it decelerates, producing a trailing ‘‘pileup’’ of dust density behind the gas density peak, which can be large. This dust-density peak then accelerates the gas, amplifying the sound wave. Because of the resonance with both drift and sound speeds, these effects add coherently as the wave propagates, leading to the exponential growth of the mode.

One further interesting feature of this mode deserves mention: the velocities ($\delta\mathbf{v} \approx \delta\mathbf{u}$ here) are not fully-aligned with $\hat{\mathbf{k}}$ but have a component in the \mathbf{k}_\perp direction,⁷ which leads the velocity in the $\hat{\mathbf{k}}$ direction by a phase angle $\sim \pi/4$. This is a response to the dust streaming in the \mathbf{k}_\perp direction and the amplitude of this term decreases with k .

(iii) **Resonant Mode, Short-Wavelengths** ($\kappa_\parallel \gg \hat{\mu}^{-1}$; Eq. (17)): At high- k with $w_s \geq 1$ the details of the resonant mode (and scaling of the growth rate) change. The resonant condition remains the same as at mid k , however, the mode propagates with wavespeed $c_s \hat{\mathbf{k}}$ along the resonant angle $\cos\theta = \pm 1/w_s$, and the gas behaves like a soundwave (the velocities are now aligned $\delta\mathbf{u} \propto \delta\mathbf{v} \propto \mathbf{k}$). This generates a strong dust response with the slightly-modified scaling $|\delta\rho_d|/|\delta\rho| \sim (4\mu\kappa_\parallel)^{1/3} \gg 1$ (scaling like the growth rate), with $\delta\rho_d$ lagging the gas mode by a phase angle $\sim \pi/6$. Importantly, $|\delta\rho_d|/|\delta\rho|$ continues to increase indefinitely with k , and in this regime, the dust density perturbation becomes *larger* than the gas density perturbation in absolute units (even though the mean dust density is smaller than gas by a factor μ). The dust velocity $\delta\mathbf{v}$ is parallel to $\delta\mathbf{u}$, but with a smaller amplitude $|\delta\mathbf{v}|/|\delta\mathbf{u}| \sim (\mu\kappa_\parallel/2)^{-1/3} \ll 1$, and $\delta\mathbf{v}$ leads $\delta\mathbf{u}$ by a phase angle $\sim \pi/6$.

4 DIFFERENT DRAG PHYSICS

In this section, we consider different physical drag laws. This involves inserting specific forms of η and ζ into the dispersion relations derived in § 3. Numerically calculated growth rates for representative cases are shown for comparison in Fig. 3. For simplicity of notation, we again use the dimensionless variables (7) throughout this section.

4.1 Constant Drag Coefficient

The simplest case is $t_s = \text{constant}$, so $\delta t_s = 0$ – i.e. $\eta = \zeta = 0$ (and $\tilde{\zeta} = 1$). The characteristic polynomial simplifies to $B_\omega = A_\omega B'_\omega$ with $B'_\omega \equiv \omega'(\omega' + i)(\omega^2 - k^2) + i\mu(\omega^2\omega' - \kappa_\parallel^2\{\omega' + i\})$. Since $\tilde{\zeta} = 1$, all pure-perpendicular modes are damped or stable.

The long-wavelength modes are unstable with growth rates,

$$\omega(\kappa_\parallel \ll \hat{\mu}) = \kappa_\parallel + \frac{\pm\sqrt{3} + i}{2} \hat{\mu}^{1/3} \kappa_\parallel^{2/3}. \quad (19)$$

For $w_s < 1$, these cut off at high- k with $\omega \approx (\mu/2)(w_s^2 - k^2/(1 + \mu^2))$ (Eq. (18)). For $w_s \geq 1$, at large k the intermediate mode (Eq. (11)) is present with growth rate $= \mu(w_s |\cos\theta| - 1)/2$ so the most rapidly-growing mode is parallel. The slow mode (Eq. (14)) is present with growth rate $\sim \mu/[1 - (w_s \cos\theta)^{-2}]$. At resonance

($\cos\theta \rightarrow \pm 1/w_s$), the growth rate is,

$$\omega_* = \begin{cases} \kappa_\parallel \left(1 - \frac{\hat{\mu}}{4}\right) - i\frac{\hat{\mu}}{8} + \frac{(1+i)}{2} (\hat{\mu}\kappa_\parallel)^{1/2} & (\hat{\mu} \ll \kappa_\parallel \ll \hat{\mu}^{-1}) \\ \kappa_\parallel - i\frac{1+\mu}{3} + (1+i\sqrt{3}) \left(\frac{\mu\kappa_\parallel}{16}\right)^{1/3} & (\kappa_\parallel \gg \hat{\mu}^{-1}). \end{cases} \quad (20)$$

4.2 Epstein Drag (Aerodynamic Particles)

The general expression⁸ for the drag in the Epstein limit is:

$$t_s = \sqrt{\frac{\pi\gamma}{8}} \frac{\bar{\rho}_d R_d}{\rho c_s} \left(1 + a_\gamma \frac{|\mathbf{v} - \mathbf{u}|^2}{c_s^2}\right)^{-1/2}, \quad a_\gamma \equiv \frac{9\pi\gamma}{128}. \quad (21)$$

Where $\bar{\rho}_d$ is the internal material density of the aerodynamic particle and R_d is the particle (grain) radius. For astrophysical dust, $\bar{\rho}_d \sim 1 - 3 \text{ g cm}^{-3}$, and $R_d \sim 0.001 - 1 \mu\text{m}$ in the ISM, or in denser environments $R_d \sim 0.1 - 1000 \mu\text{m}$ (e.g., protoplanetary disks, SNe ejecta, or cool star atmospheres; Draine 2003). Note that Epstein drag depends on the *isothermal* sound speed, $c_{\text{iso}} \equiv \sqrt{k_B T/m_{\text{eff}}}$ (where m_{eff} is the mean molecular weight). However, because we work in units of the sound speed $c_s \equiv \sqrt{\partial P/\partial \rho}$, we relate the two via the usual equation-of-state parameter γ ,

$$\gamma \equiv \frac{c_s^2}{c_{\text{iso}}^2} = \frac{\rho}{P} \frac{\partial P}{\partial \rho}, \quad (22)$$

and will assume γ is a constant under linear perturbations.

Note that because t_s now depends on $\langle |\mathbf{v} - \mathbf{u}| \rangle = |\mathbf{w}_s|$, Eq. (2) for the drift velocity, $\mathbf{w}_s = \mathbf{a} \langle t_s \rangle / (1 + \mu)$, is implicit. Define $w_{s,0} \equiv |\mathbf{a}| t_0 / (c_s (1 + \mu))$ where $t_0 \equiv (\pi\gamma/8)^{1/2} \bar{\rho}_d R_d / (\rho_0 c_s)$ is the stopping time at zero relative velocity. Then the solution of Eq. (2) is

$$w_s^2 = \frac{1}{2a_\gamma} \left[(1 + 4a_\gamma w_{s,0}^2)^{1/2} - 1 \right], \quad (23)$$

which reduces to $w_s \approx w_{s,0}$ for $|\mathbf{a}| \ll c_s/t_0$, or $w_s \approx a_\gamma^{-1/4} w_{s,0}^{1/2}$ for $|\mathbf{a}| \gg c_s/t_0$.

With Eq. (21) for t_s and Eq. (23) for w_s , δt_s follows Eq. (5) with

$$\eta = \frac{\gamma + 1 + 2a_\gamma w_s^2}{2(1 + a_\gamma w_s^2)}, \quad \zeta = \frac{a_\gamma w_s^2}{1 + a_\gamma w_s^2}. \quad (24)$$

From this we can derive the relevant instability behavior for different γ and w_s . Note $\eta > 0$ and $\zeta > 0$, so the ‘‘decoupling’’ instability (which required $\tilde{\zeta} < 0$) is not present.

4.2.1 Super-sonic streaming ($w_s \gg 1$)

In the $w_s \gg 1$ limit, $\eta \rightarrow 1 + \mathcal{O}(w_s^{-2})$ (independent of γ) and $\zeta \rightarrow 1$. This stabilizes the intermediate modes (Eq. (11)) because at high- w_s , the ζ term dominates over $(1 - \eta)$, viz., the stronger coupling from at high relative velocity stabilizes the modes. The long-wavelength modes (Eq. (10)) are present and saturate in the slow/resonant mode, with maximum growth rate $\Im(\omega) \sim \mu[1 - (w_s \cos\theta)^{-2}]^{-1} (1 - \eta/\zeta)$, which approaches $\Im(\omega) \sim \mu/2$ for $w_s \gg 1$ out-of-resonance.

⁸ Equation (21) is actually a convenient polynomial approximation, given in Draine & Salpeter (1979), to the more complicated dependence on $|\mathbf{v} - \mathbf{u}|$. However using the more complicated expression yields negligible ($\sim 1\%$) differences for any parameters considered here.

⁷ Note that for $w_s \gg 1$, the \mathbf{k}_\perp direction is approximately the $\hat{\mathbf{w}}_s$ direction.

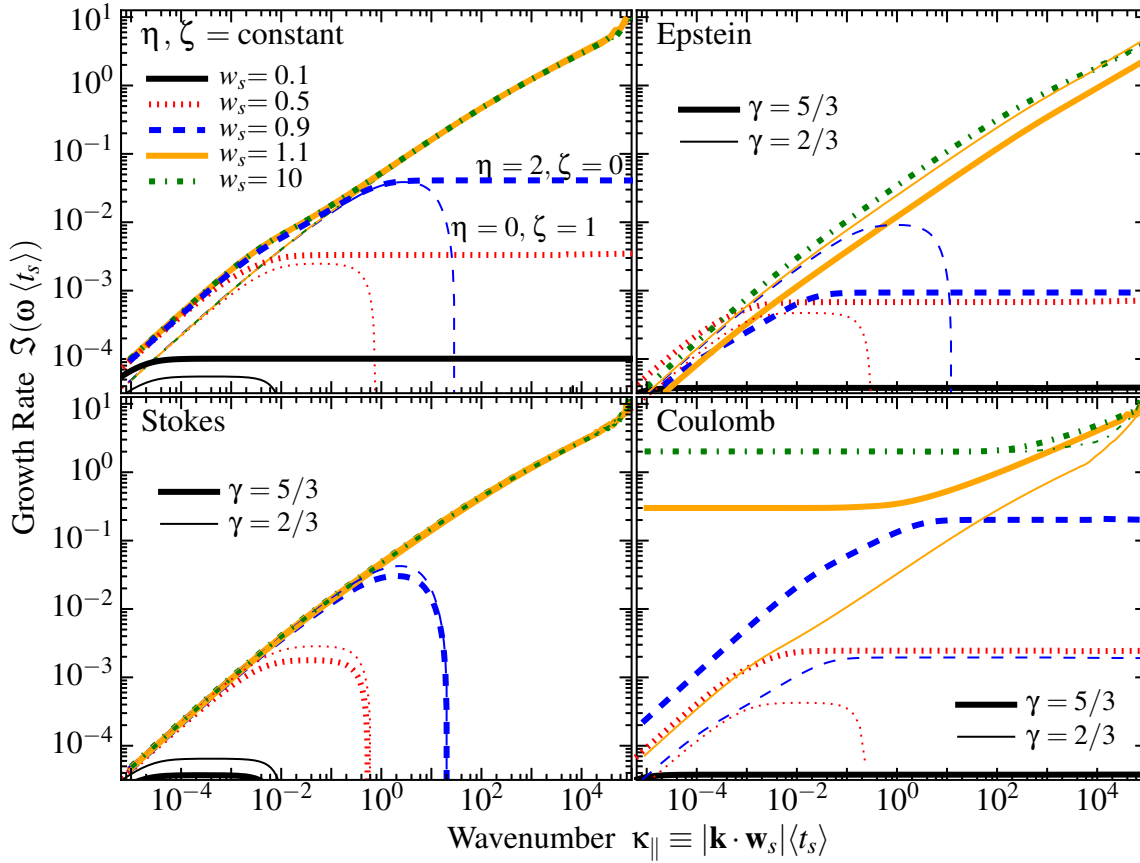


Figure 3. Growth rates of the most-rapidly-growing unstable mode as a function of wavenumber and drift velocity, as Fig. 1, for different drag laws (see § 4). Here we take $\mu = 0.01$, $\phi = 0$, and marginalize over angle (the most rapidly-growing cases $\cos\theta = 1$ for $w_s < 1$ or $\cos\theta = \pm 1/w_s$ for $w_s \geq 1$). *Top Left:* Arbitrary constant η , ζ parameterization of t_s (Eq. (5)) with $\eta = 2$, $\zeta = 0$ (thick lines) or $\eta = 0$, $\zeta = 1$ (thin lines). As shown in § 3 the dependence on these parameters is weak; the largest effect is to determine, when $w_s < 1$, whether all k are unstable (if $\eta > 1 + \zeta$) or only small- k ($\eta < 1 + \zeta$), but the maximum growth rates in these cases are very similar. *Top Right:* Epstein drag (§ 4.2), with gas equation-of-state parameters $\gamma = 5/3$ (thick) or $\gamma = 2/3$ (thin). The qualitative behavior is identical, with modest normalization differences, and the transition between regimes for $w_s < 1$ ($\eta = 1 + \zeta$) occurring at $\gamma^{-1} = 1 - 9\pi w_s^2/64$ (η , ζ depend on γ and w_s). Note the low saturation value of the $\gamma = 5/3$, $w_s = 0.9$ case occurs because it is very close to this singular value ($(1 + \zeta) - \eta \approx 0.02$). *Bottom Left:* Stokes drag (§ 4.3). The dependence on γ is weak and for all $\gamma < 3$, high- k modes with $w_s < 1$ are stable. *Bottom Right:* Coulomb drag (§ 4.4; here $\Gamma = 1$). For long-wavelength modes with $w_s < 1$, and all high-wavelength modes, the qualitative behavior is similar to other laws although normalization differences are more obvious. The high growth-rate, low- k modes with $w_s > 1$ are a different instability which manifests because when $w_s > 1$ in Coulomb drag, increasing the dust-gas velocity *decreases* the drag acceleration, so the dust speeds up and the system “self-decouples.” Physically Epstein or Stokes drag should be dominant over Coulomb drag in this limit.

At resonance, we insert the full expressions for η and ζ into Eq. (16) and Eq. (17). This gives

$$\omega_* \approx k \varpi_{\Re} - \frac{i\hat{\mu}}{8} \left(\frac{\tilde{\zeta} - \eta}{\tilde{\zeta}} \right) + \frac{i\pm 1}{2} \left(\left| \frac{\tilde{\zeta} - \eta}{\tilde{\zeta}} \right| \hat{\mu} k \right)^{1/2}, \quad (25)$$

$$\frac{\tilde{\zeta} - \eta}{\tilde{\zeta}} = \frac{1 + 2a_\gamma w_s^2 - \gamma}{2 + 4a_\gamma w_s^2} = \frac{1}{2} + \mathcal{O}(w_s^{-2}),$$

$$\varpi_{\Re} = 1 + \frac{3\hat{\mu}}{16} \left(1 + \mathcal{O}(w_s^{-2}) \right),$$

in the “mid- k ” regime (we show the lowest order terms in w_s^{-1} for simplicity), and

$$\omega_* \approx k - i\varpi + (i\sqrt{3} + 1) \left(\frac{|\Theta| \mu k}{16} \right)^{1/3} \quad (26)$$

$$\Theta = \frac{1 - \gamma + 2a_\gamma}{2(1 + a_\gamma w_s^2)} = \frac{1 - \gamma + 2a_\gamma}{2a_\gamma w_s^2} + \mathcal{O}(w_s^{-4}),$$

$$\varpi = -\frac{2a_\gamma w_s^2}{3(1 - \gamma + 2a_\gamma)} + \mathcal{O}(w_s^0),$$

in the “high- k ” regime. We see that in the mid- k regime, the growth

rate is mostly independent of w_s and γ , while in the high- k regime the growth rate decreases, $\Im(\omega_*) \propto w_s^{-2/3}$, at large w_s .

The dependence on γ is weak. At mid k , we see from Eq. 25 that the growth rate declines as we approach the point where $\tilde{\zeta} - \eta = 0$, which occurs at $w_s^2 = 64(\gamma - 1)/(9\pi\gamma)$. This implies that unless the gas equation of state is very stiff – specifically, $\gamma > 64/(64 - 9\pi) \approx 1.8$ – this “stable point” does not exist for $w_s > 1$ (a necessary condition for resonant modes). Even for $\gamma \gtrsim 1.8$, the point of stability occurs only at a specific w_s , and so is unlikely to be of physical significance.

At high- k , we see somewhat similar behavior, with the growth rate declines as γ approaches the point where $\Theta = 0$ (and ϖ diverges), at $\gamma = 64/(64 - 9\pi) \approx 1.8$. In fact, at this point exactly, our series expansion is incorrect (since ϖ diverges), and a resonant mode still exists, but with a growth rate that increases more slowly with k :

$$\omega_* = k + \left(\sin \frac{\pi}{8} + i \cos \frac{\pi}{8} \right) \left(\frac{(w_s^2 - 1)a_\gamma \mu k}{2(1 + a_\gamma w_s^2)} \right)^{1/4}. \quad (27)$$

Again, it seems unlikely that this specific point, $\gamma \approx 1.8$ is of par-

ticular physical significance (and in any case, the system is still unstable, just with the reduced growth rate (27)).

4.2.2 Sub-Sonic ($w_s \ll 1$)

Now consider $w_s \ll 1$. In this limit $\eta = (\gamma + 1)/2 + \mathcal{O}(w_s^2)$ and $\zeta = a_\gamma w_s^2 + \mathcal{O}(w_s^4)$; i.e., the velocity-dependent terms in t_s become second-order, as expected. For $w_s < 1$ the resonant and intermediate modes are stabilized. We also see that the type of unstable mode will depend on the value of γ : if $\gamma > 1$ then $\eta/\tilde{\zeta} \approx (\gamma + 1)/2 > 1$, which implies the “slow subsonic” mode at low- k from Eq. (18) is stabilized, but “slow” mode from Eq. (14) is unstable; if $\gamma < 1$, the “slow” mode at $k \gtrsim 1$ becomes damped at high k , and the “slow subsonic” low- k expression from Eq. (18) is unstable.

The “slow” modes, relevant for $\gamma \gtrsim 1$, have growth rates that increase with k for $k \ll \hat{\mu}$ (the long-wavelength mode; Eq. (10)), then saturate to a constant maximum for $k \gtrsim 1$ (i.e. all modes shorter-wavelength than the length scale $\sim c_s \langle t_s \rangle$ have similar growth rate). For large k and $w_s \ll 1$ the growth rate from Eq. (14) is $\Im(\omega) \approx w_s^2 \cos^2 \theta \mu (\gamma - 1)/2$. The “slow subsonic” mode (Eq. (18)), relevant for very soft equations of state with $\gamma \lesssim 1$, has a maximum growth rate $\Im(\omega) \approx w_s^2 \mu (\tilde{\zeta} - \eta)/2 \approx w_s^2 \mu (1 - \gamma)/4$, which again occurs for parallel modes. The mode is stabilized at short wavelengths, $k \gtrsim (1 + \mu)w_s \sqrt{1 - \gamma}$.

Overall, we see that for *all* γ , there is an unstable parallel mode at low $w_s \ll 1$, with maximum growth rate $\sim w_s^2 \mu$. The difference is that for $\gamma > 1$ the unstable modes are slow modes, which are unstable at all k and propagate with velocity \mathbf{w}_s when $k \gg 1$; for $\gamma < 1$ the instability only exists for long wavelength modes $k \lesssim w_s$, which propagate with velocity $\pm c_s \hat{\mathbf{w}}_s / \sqrt{1 + \mu}$.

Again there is one critical point when $\tilde{\zeta} - \eta = 0$, or $w_s^2 = 64(\gamma - 1)/(9\pi\gamma)$, where the standard long-wavelength instability vanishes. This occurs only for some specific w_s at a given γ , so is unlikely to be of physical significance. Again, at this point, there is in fact still an instability, albeit with a reduced growth rate (see footnote 2, near Eq. (10); the instability only truly vanishes at $\zeta = 0$, $\eta = 1$ exactly).

4.3 Stokes Drag

The expression for drag in the Stokes limit – which is valid for an intermediate range of grain sizes, when $R_d \gtrsim (9/4)\lambda_{\text{mfp}}$ but $\text{Re}_{\text{grain}} \equiv R_d |\mathbf{w}_s| / (\lambda_{\text{mfp}} c_s) \lesssim 1$ – is given by multiplying the Epstein expression (Eq. (21)) by $(4R_d)/(9\lambda_{\text{mfp}})$. Here $\lambda_{\text{mfp}} \propto 1/(\rho\sigma_{\text{gas}})$ is the gas mean-free-path, σ_{gas} is the gas collision cross section, and Re_{grain} is the Reynolds number of the streaming grain.

We can solve implicitly for the dust streaming velocity \mathbf{w}_s , which is the same as in the Epstein case (since t_s depends on $|\mathbf{v} - \mathbf{u}|$ in the same manner). However, the absolute value of t_s only determines our units, and the behavior of interest depends only on the coefficients η and ζ . Since R_d is a material property of the dust and σ_{gas} an intrinsic property of the gas, the important aspect of the Stokes drag law is that it multiplies the Epstein law by one power of ρ . Although it is certainly possible σ_{gas} might depend on density and/or temperature, lacking a specific physical model for this we will take it to be a constant for now. This simply gives $\eta \rightarrow \eta - 1$, relative to the scalings for Epstein drag.

When $w_s \ll 1$ (c.f., § 4.2.2 for Epstein drag), $\eta = (\gamma - 1)/2 + \mathcal{O}(w_s^2)$ and $\zeta = a_\gamma w_s^2 + \mathcal{O}(w_s^4)$, and intermediate and resonant modes are stabilized (because $w_s < 1$). The slow (high- k) mode is stabilized for $1 - \eta/\tilde{\zeta} \approx (3 - \gamma)/2 > 0$, viz., so as long as $\gamma < 3$ (which is expected in almost all physical situations) the slow mode is damped. However for all $\gamma < 3$, the slow-subsonic low- k mode (Eq. (18)) is unstable for $k \lesssim w_s$, with maximum growth rate

$\Im(\omega) \approx w_s^2 \mu (3 - \gamma)/4$. This is larger (smaller) than the Epstein drag growth rate for $\gamma < 5/3$ ($\gamma > 5/3$).

In the limit $w_s \gg 1$, the Stokes drag expression cannot formally apply because $R_d > \lambda_{\text{mfp}}$ then implies $\text{Re}_{\text{grain}} = R_d |\mathbf{w}_s| / (\lambda_{\text{mfp}} c_s) \gtrsim 1$. When this is the case, either because w_s is large or (more commonly) R_d is large, there is no longer a simple drag law because the grain develops a turbulent wake. This will tend to increase the drag above the Stokes estimate (the turbulence increases the drag) with a stronger and stronger effect as Re_{grain} increases. Given some empirically determined scaling of t_s with R_d , ρ , w_s etc. (see, e.g., Clair et al. 1970 for subsonic drag), one could still qualitatively consider such a turbulent drag within the framework above, with the properties of the turbulence determining η and ζ . We do not do this here, but note that because Re_{grain} increases with w_s and ρ (through λ_{mfp}), we expect t_s to decrease with w_s and ρ , viz., $\eta > 0$ and $\zeta > 0$. The general scalings are thus likely similar to the Epstein case, but with a larger ζ for $w_s \ll 1$, because the velocity dependence of the drag will be significant, even for subsonic streaming.

Of course we can still simply calculate what the mode growth rates would be, if the usual Stokes expression applied even for $w_s \gtrsim 1$. This is shown in Fig. 3, for the sake of completeness.

4.4 Coulomb Drag

The standard expression⁹ for t_s in the Coulomb drag limit is

$$t_s = \sqrt{\frac{\pi\gamma}{2}} \frac{\bar{\rho}_d R_d}{\rho c_s \ln \Lambda} \left(\frac{k_B T}{z_i e U} \right)^2 \left[1 + ac \frac{|\mathbf{v} - \mathbf{u}|^3}{c_s^3} \right] \quad (28)$$

$$\Lambda \equiv \frac{3k_B T}{2R_d z_i e^2 U} \sqrt{\frac{m_i k_B T}{\pi \rho}} \quad , \quad ac \equiv \sqrt{\frac{2\gamma^3}{9\pi}}$$

where $\ln \Lambda$ is the Coulomb logarithm, e is the electron charge, z_i is the mean gas ion charge, m_i is the mean molecular weight, $T \propto \rho^{\gamma-1}$ is the gas temperature, and U is the electrostatic potential of the grains, $U \sim Z_{\text{grain}} e / R_d$ (where Z_{grain} is the grain charge). The behavior of U is complicated and depends on a wide variety of environmental factors: in the different regimes considered in Draine & Salpeter (1979) they find regimes where $U \sim \text{constant}$ and others where $U \propto Z_{\text{grain}} \propto T$, we therefore parameterize the dependence by $U \propto T^\Gamma$.

With this ansatz, we obtain

$$\eta = 1 + 2(\gamma - 1)\Gamma - \frac{3(\gamma - 1)}{2(1 + ac w_s^3)} - \frac{1 - (3 - 2\Gamma)(\gamma - 1)}{2 \ln \Lambda},$$

$$\zeta = -\frac{3ac w_s^3}{1 + ac w_s^3} < 0. \quad (29)$$

For relevant astrophysical conditions, $\ln \Lambda \sim 15 - 20$, so the $\ln \Lambda$ term in η is unimportant.

In general, Coulomb drag is sub-dominant to Epstein or Stokes drag under astrophysical conditions when the direct effects of magnetic fields on grains (i.e., Lorentz forces) are not important. Nonetheless, the qualitative structure of the scaling produces similar features to the Epstein and Stokes drag laws, and we consider it here for completeness. In fact, grains influenced by Coulomb drag are significantly “more unstable” than those influenced by Epstein or Stokes drag. For $w_s \ll 1$, $\eta \rightarrow [(3\gamma - 4) + (5 - 3\gamma) \log \Lambda] / (2 \log \Lambda) \approx (5 - 3\gamma)/2$ if $\Gamma = 0$, and $\eta \rightarrow$

⁹ Again, Eq. (28) is a polynomial approximation for more complex dependence on $|\mathbf{v} - \mathbf{u}|$, given in Draine & Salpeter (1979). However using this approximation versus the full expression makes no important difference to our results.

$[(\gamma - 2) + (1 + \gamma) \log \Lambda] / (2 \log \Lambda) \approx (1 + \gamma) / 2$ if $\Gamma = 1$. Since $\zeta \rightarrow 1$, the “slow” mode is unstable if $\eta > 1$ (for $\Gamma = 0$ this requires $\gamma < (-4 + 3 \log \Lambda) / (3(-1 + \log \Lambda)) \approx 0.98$; for $\Gamma = 1$ this requires $\gamma > (2 + \log \Lambda) / (1 + \log \Lambda) \approx 1.05$). As noted above for the Epstein case (§ 4.2.2), because $\zeta \rightarrow 0$ at small w_s , the scaling of the “slow subsonic” low- k mode is essentially reversed from the “slow” high- k mode: when the “slow” mode is stable at high- k ($\eta < 1$) the “subsonic” mode is unstable at low- k , and when the “slow” mode is unstable ($\eta > 1$) the “subsonic” mode is stable. In either case, whichever of the two is unstable has growth rate $\Im(\omega) \sim w_s^2 \mu |\eta| / 2$.

For $w_s \gg 1$, the drag force *decreases* rapidly for $|\mathbf{v} - \mathbf{u}| \gg c_s$ (i.e. $\zeta \lesssim -1$ when $w_s \gg 1$). In this regime, one never expects Coulomb drag to dominate over Epstein drag (which becomes more tightly-coupled at high w_s), but we consider it for completeness. We see that $\eta \approx 1$ for $\Gamma = 0$, and $\eta \approx 2\gamma - 1$ for $\Gamma = 1$. More importantly, $\zeta \rightarrow -3$. This produces the fast-growing “decoupling instability” (§ 3.3), which affects *all* wavenumbers and has a growth rate $\Im(\omega) \approx -\zeta(1 + \mu) \approx 2(1 + \mu)$. These modes arise from decoupling of the gas and dust: if the dust starts to move faster relative to the gas, t_s increases (the coupling becomes weaker), so the terminal/relative velocity increases further, and so on. If we ignore the decoupling mode, we see that each of the other modes we have discussed are still present: the high- k resonant mode (Eq. (17)) has $\Theta = (4 - 3\gamma) / (2 \log \Lambda)$ for $\Gamma = 0$ and $\Theta \approx 2(1 - \gamma)$ for $\Gamma = 1$.

5 NON-LINEAR BEHAVIOR & TURBULENCE

The non-linear behavior of the coupled dust-gas system is complex and chaotic, and will be studied in future work with numerical simulations (Moseley et al., in prep.). Here, we briefly speculate on some possible saturation mechanisms of the acoustic RDI and subsonic instabilities.

For $w_s \geq 1$, the resonant mode at the shortest wavelengths will grow fastest, with the dust density aligning locally into crests at the phase peaks with orientation $\cos \theta = \pm 1 / w_s$. These will launch small-scale perturbations in the transverse directions in the gas. Because it is short-wavelength, we do not expect the modes to be coherent on large scales, so this will drive small-scale turbulence in the gas in the transverse directions, while in the $\hat{\mathbf{w}}_s$ direction, the modes will be stretched by the drift. For $w_s < 1$, the modes grow more slowly, and, depending on η and ζ (see § 3.8), either saturate to a constant growth rate or turn over above a critical $k \gtrsim w_s$. Thus, most of the power on large scales will be in modes of order this wavelength ($k^{-1} \sim c_s^2 / (\mu |\mathbf{a}|)$). If $\mu \ll 1$, dust will go strongly non-linear before the gas does, but eventually the non-linear terms will likely lead to turbulence in the gas and dust, at least for μ not too small. Gas turbulence can then enhance dust-to-gas fluctuations (see e.g. numerical experiments with dust in super-sonic turbulence in Hopkins & Lee 2016; Lee et al. 2016). Eventually sharp dust-filaments will form, and as the modes grow beyond this point, dust trajectories will cross and the fluid approximation for the dust will break down. Rayleigh-Taylor type secondary instabilities will likely appear, as regions with higher gas density are accelerated more rapidly, while those without dust are not dragged efficiently. It also seems possible that for $\mu \ll 1$ and/or w_s not very large, the modes saturate in a laminar way (e.g., by changing shape, or if the dust fluid approximation breaks down).

We can crudely guess the saturation amplitude of the non-linear turbulence by comparing the energy input from the imposed acceleration (without including the bulk acceleration of the sys-

tem),

$$\frac{dE_{\text{accel}}}{dt} \sim \frac{d}{dt} (m_{\text{dust}} v_{\text{dust-gas}}^2) \sim m_{\text{dust}} \langle \mathbf{v}_{\text{dust-gas}} \rangle \cdot \mathbf{a} \sim \frac{\mu |\mathbf{w}_s|^2}{\langle t_s \rangle}, \quad (30)$$

to the energy decay rate of turbulence

$$\frac{dE_{\text{turb}}}{dt} \sim -(m_{\text{gas}} + m_{\text{dust}}) \frac{v_{\text{eddy}}^2}{t_{\text{eddy}}} \sim -(1 + \mu) \frac{\delta v_{\text{sat}}^3}{\lambda}, \quad (31)$$

where λ is the driving scale. Equating (30) and (31) gives $\delta v_{\text{sat}} \sim (\hat{\mu} |\mathbf{w}_s|^2 \lambda_{\text{drive}} / \langle t_s \rangle)^{1/3}$. For each range of the RDI, we can then equate the turbulent dissipation rate $t_{\text{diss}}^{-1} \sim t_{\text{eddy}}^{-1} \sim v_{\text{eddy}} / \lambda \sim (\mu |\mathbf{w}_s|^2 / \langle t_s \rangle)^{1/3} \lambda^{-2/3}$ to the growth rate $\Im(\omega)$, which should (in principle) allow for the estimation of a characteristic scale and saturation amplitude in the resulting turbulence. However, one finds that: (i) in the low- k regime, with $\Im(\omega) \sim (\hat{\mu} / \langle t_s \rangle)^{1/3} (|\mathbf{w}_s| k)^{2/3}$, the two are identical and there is no obvious characteristic λ ; (ii) in the mid- k regime, with $\Im(\omega) \sim (\hat{\mu} c_s k / \langle t_s \rangle)^{1/2}$, the characteristic scale is $\lambda / (c_s \langle t_s \rangle) \sim w_s^4 \hat{\mu}^{-1}$, which is outside of the range of validity of the mid- k regime; and (iii) in the high- k regime, with $\Im(\omega) \sim (\hat{\mu} c_s k / \langle t_s \rangle)^{1/3}$, the characteristic scale is $\lambda / (c_s \langle t_s \rangle) \sim w_s^2$, which is outside of the range of validity of the high- k regime (if $\hat{\mu} < 1$). Thus, we see that there is no obvious way for the system to choose a scale for resonant modes in *any* wavelength regime. What we instead expect is that turbulence will begin on small scales and grow to larger and larger λ , up to the scale of the system (if the given sufficiently long time periods). One might also expect that this the characteristic scale would increase in time, in some way proportional to the growth rate at a given λ . This suggests that $\lambda \sim t^3$ ($\delta v \sim t$) at early times (with the instability growing in the high- k regime), $\lambda \sim t^2$ ($\delta v \sim t^{2/3}$) at intermediate times (in the mid- k regime), then slowing to $\lambda \sim t^{3/2}$ ($\delta v \sim t^{1/2}$) at longer times (in the long-wavelength regime).¹⁰ This qualitative behavior – viz., turbulence that moves to larger and larger scales as a function of time – is observed in simulations of cosmic-ray-driven instabilities, which have some similar characteristics to the dust-gas instabilities studied here (see, e.g., Riquelme & Spitkovsky 2009; Matthews et al. 2017).

6 SCALES WHERE OUR ANALYSIS BREAKS DOWN

We now briefly review the scales where our analysis breaks down.

(i) **Non-Linearity & Orbit-Crossing:** If there is sufficiently sharp structure in the velocity or density fields, the dust trajectories become self-intersecting and the fluid approximation is invalid (for dust). In this limit numerical simulations must be used to integrate particle trajectories directly. This should not occur in the linear regime (see App. A of Jacquet et al. 2011 for more discussion).

(ii) **Smallest Spatial Scales:** At sufficiently short wavelengths (high k) approaching the gas mean-free-path, dissipative effects will be important.¹¹ For ionized gas, this scale is $\lambda_{\text{mfp}}^{\text{gas}} \sim 10^{12} \text{ cm} (T / 10^4 \text{ K})^2 (n_{\text{gas}} / \text{cm}^{-3})^{-1}$. If we assume Epstein drag with modest $w_s \sim 1$, this gives a dimensionless $\kappa_{\text{max}} \sim (2\pi c_s \langle t_s \rangle / \lambda_{\text{mfp}}) \sim 10^9 (R_d / \mu \text{ m}) (T / 10^4 \text{ K})^{-2} \gg 1$.

¹⁰ Of course, actually resolving this shift in simulations would generally require an unfeasibly large dynamic range.

¹¹ More precisely, the fluid viscosity is important when $\omega u \sim \nu_{\text{vis}} k^2 u$, where u is the perturbed gas velocity, and $\nu_{\text{vis}} \sim c_s \lambda_{\text{mfp}}^{\text{gas}}$ is the kinematic viscosity. For $\omega \sim c_s k$, as is the case for the RDI (it is a perturbed sound wave), we find that viscosity is important when $k \sim 1 / \lambda_{\text{mfp}}^{\text{gas}}$.

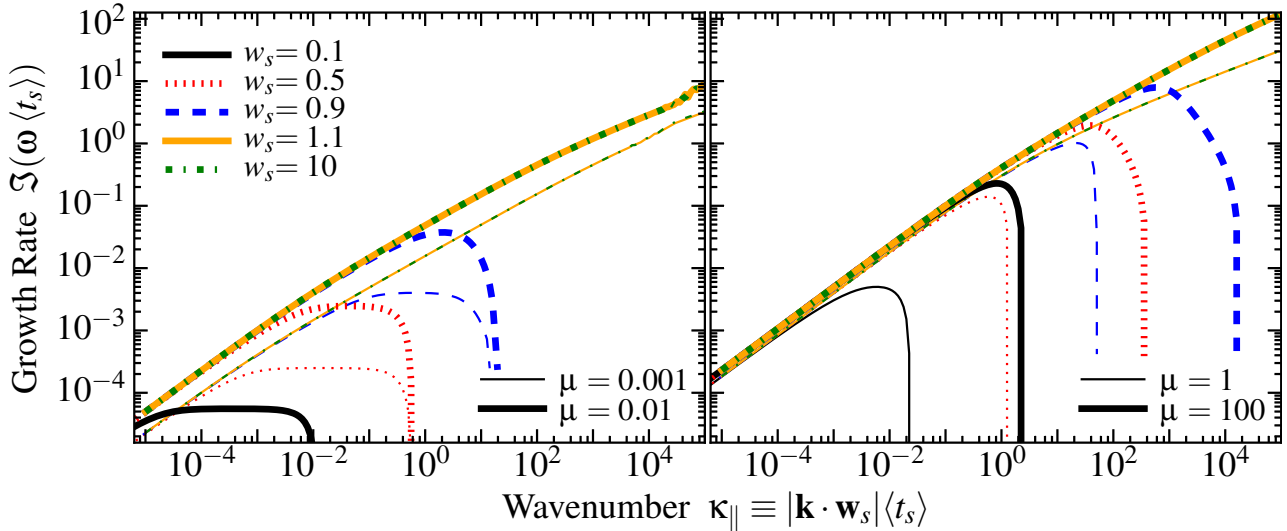


Figure 4. Growth rates of the most-rapidly-growing unstable mode as a function of wavenumber and drift velocity, as Fig. 1, for different dust-to-gas ratios $\mu = 0.001, 0.01, 1, 100$ (the $\mu = 0.01$ case is in Fig. 1). For simplicity we take a constant drag coefficient ($\eta = \zeta = \phi = 0$, as Fig. 1), and marginalize over angle at each κ_{\parallel} . As shown in § 3, the dependence on μ at a given κ_{\parallel} is quite weak. At low $\mu \ll 1$, the low and high- k growth rates scale $\propto \mu^{1/3}$, with the slightly stronger $\propto \mu^{1/2}$ dependence around $\kappa_{\parallel} \sim 1$. At large $\mu \gtrsim 1$, the low and intermediate- k growth rates become independent of μ (because they scale with $\hat{\mu} \equiv \mu/(1+\mu) \rightarrow 1$ for large μ); the high- k growth rate continues to increase weakly with $\mu^{1/3}$. In the sub-sonic ($w_s < 1$) case, however, the maximum wavenumber where the growth rate either saturates or the mode becomes stable increases with μ so that the maximum growth rate (marginalizing over k) increases roughly $\propto \mu^{2/3}$. For the super-sonic ($w_s > 1$) case all wavelengths are unstable independent of μ , so there is no such dependence.

In the dust, the fluid approximation breaks down on scales comparable to the dust-particle separation $\lambda_{\text{sep}}^{\text{dust}} \sim 10^5 \text{ cm} (R_d/\mu m) (n_{\text{gas}}/1 \text{ cm}^{-3})^{-1/3} (\mu/0.01)^{-1/3}$, which is much smaller than $\lambda_{\text{mfp}}^{\text{gas}}$ under most astrophysical conditions. Because each of these minimum scales (for the gas and the dust) are small, very small wavelengths (e.g., up to $\kappa_{\parallel} \sim k_{\text{max}} c_s \langle t_s \rangle \sim 10^9$ in Figs. 1, 3, and 4) are astrophysically relevant.

(iii) **Largest Spatial Scales:** At low k , we eventually hit new scale lengths (e.g. the gas pressure-scale-length). The physical scale where $\kappa_{\parallel} \sim 1$, i.e., where $k \sim c_s \langle t_s \rangle$, can be large. For example, with Epstein drag at $w_s \sim 1$ this is $k^{-1} \sim 10^{20} \text{ cm} (R_d/\mu m) (n_{\text{gas}}/\text{cm}^{-3})^{-1}$. For dust in AGN torii, starburst regions, or GMCs affected by massive stars, this is only ~ 100 times smaller than the system scale, so the long-wavelength instability ($k c_s \langle t_s \rangle \ll \mu$) will likely require a global analysis. However, in cool stars the densities are much higher and the scales correspondingly smaller; e.g., for $\rho \sim \rho_{-12} 10^{-12} \text{ g cm}^{-3}$ we obtain $k_{\text{min}} c_s \langle t_s \rangle \sim 10^{-5} (R_{\text{min}}/100 R_{\text{sun}})^{-1} (R_d/\mu m) \rho_{-12}^{-1}$ (see § 8 for more details).

(iv) **Maximum Timescales:** Dust with speed $|\mathbf{w}_s|$ will drift through a system of size R_0 on a timescale $\sim R_0/|\mathbf{w}_s|$. An instability must grow faster than this to be astrophysically relevant.

7 RELATION TO PREVIOUS WORK

7.1 Winds from Cool Stars

In the context of dust-driven winds from red giants and other cool stars, there has been extensive work on other dust-related instabilities (involving thermal instability, dust formation, Rayleigh-Taylor instabilities, magnetic cycles, etc; see MacGregor & Stencil 1992; Hartquist & Havnes 1994; Sandin & Höfner 2003; Soker 2000, 2002; Simis et al. 2001; Woitke 2006a,b), but these are physically distinct from the instabilities studied here. Of course, simulations with the appropriate physics – namely, (1) explicit integration of

a drag law with gas back-reaction, (2) trans-sonic w_s , (3) multi-dimensional (2D/3D) domains, and (4) sufficient resolution (for the high- k resonant modes) – should see the RDI. Most studies to date to not meet these conditions. Moreover they often include other complicated physics (e.g. opacity and self-shielding, dust formation) which are certainly important, but make it difficult to identify the specific instability channel we describe here.

However, some authors have previously identified aspects of the instabilities described above. Morris (1993) performed a much simpler linear stability analysis on a two-fluid mixture subject to drag (see also Mastrodemos et al. 1996), and noted two unstable solutions whose growth rates saturated at high- k : these are the “slow” and “intermediate” modes identified here. However, they assumed: (1) zero gas pressure (effectively $w_s \rightarrow \infty$), preventing identification of stability criteria; (2) a constant coupling coefficient; and (3) spherical symmetry (of the perturbations) which eliminates the resonant mode. Deguchi (1997) followed this up allowing for non-zero gas pressure, but retaining spherical symmetry and imposing the assumption that the dust always exactly follows the local equilibrium drift velocity. This suppresses all instabilities except the resonant mode at $w_s = c_s$ exactly. To our knowledge, the scaling of these instabilities and the existence of the resonant instability for all k and all $w_s > 1$ has not been discussed previously in the literature.

7.2 Starburst and AGN Winds

In models of starbursts and AGN, there is a long literature discussing radiation pressure on grains as an acceleration mechanism for outflows or driver of turbulence (see e.g. Heckman et al. 1990; Scoville et al. 2001; Thompson et al. 2005; Krumholz & Matzner 2009; Hopkins & Elvis 2010; Hopkins et al. 2011; Murray et al. 2010; Kuiper et al. 2012; Wise et al. 2012). But almost all calculations to date treat dust and gas as perfectly-coupled (so the RDI cannot appear). The RDI is not related to the “radiative Rayleigh-Taylor” instability of a radiation pressure-supported gas+dust fluid (Krumholz & Thompson 2012; Davis et al. 2014), or non-linear hydrodynamic instabilities generated by e.g. pressure gradients or en-

tropy inversions ultimately sourced by dust “lifting” material (e.g. Berruyer 1991), nor the dust sedimentation effects in ambipolar diffusion in molecular clouds discussed in Cochran & Ostriker (1977); Sandford et al. (1984). Each of these other classes of instability do not involve local dust-to-gas ratio fluctuations.

There recently has been more work exploring dust-gas decoupling in molecular cloud turbulence and shocks (integrating the explicit dust dynamics; see Hopkins & Lee 2016; Lee et al. 2016; Monceau-Baroux & Keppens 2017) which has shown this can have important effects on cooling, dust growth, and star formation. However, these studies did not identify instabilities, or include the necessary physics to capture the RDI.

7.3 Proto-Planetary Disks

There has been extensive study of dust-gas instabilities in protoplanetary disks (Bracco et al. 1999; Cuzzi et al. 2001; Youdin & Goodman 2005; Johansen & Youdin 2007; Carballido et al. 2008; Bai & Stone 2010a,b; Pan et al. 2011; Dittrich et al. 2013; Jalali 2013; Hopkins 2016). As illustrated in SH, many of these are in fact examples of the general class of RDI (although this has not been noted before in this context). However in these cases the mode with which the dust “resonates” is not a sound wave, but some other mode (e.g. epicyclic oscillations in the case of the “streaming instability”; Youdin & Goodman 2005), which leads to distinct behavior. The acoustic RDI has not been explored in this literature.

7.4 Plasma Instabilities

As noted in SH, the most general RDI is closely related to instabilities of two-fluid plasmas (see, e.g., Tytarenko et al. 2002 for an in-depth analysis of a closely related coupled neutral gas-MHD instability). These include the Wardle (1990) instability and cosmic ray streaming instabilities (Kulsrud & Pearce 1969; Bell 2004). However, these are quite distinct physical systems and the instabilities have different linear behaviors.

8 ASTROPHYSICAL APPLICATIONS

There are a number of astrophysical contexts where this specific example of the SH instability may be important, which we review here. In the discussions below, we estimate the radiative acceleration of the dust from $\mathbf{a} \sim \mathbf{F}_\lambda Q_\lambda \bar{\rho}_d / (cR_d)$, where $|\mathbf{F}_\lambda| \sim L/R^2$ is the incident flux of radiation from a source of luminosity L and size R , c is the speed of light, and Q_λ is the radiative efficiency ($Q_\lambda \sim 1$ for very large grains, $Q_\lambda \propto R_d$ for smaller grains; see § 2.3.2)

(i) **AGN-Driven Outflows and the AGN “Torus”:** Around a luminous AGN, gas and dust are strongly differentially accelerated by radiation pressure. There is some dust sublimation radius close to the AGN, interior to which dust is destroyed. The instabilities must occur outside this region in the dusty “torus,” or further out still, in the galactic narrow-line region.

If we assume the AGN has luminosity $L \sim L_{46} 10^{46} \text{ erg s}^{-1}$, with a torus radius external to the dust sublimation radius $R \sim 0.3 \text{ pc } L_{46}^{1/2}$ and midplane column density $\sim n_{\text{gas}} R \sim N_{26} 10^{26} \text{ cm}^{-2}$, and Epstein drag with a gas temperature $T \sim 100 \text{ K}$ (see Eq. 23), we find we are in the highly super-sonic limit with $w_s \gtrsim 100 L_{46}^{1/4} N_{26}^{-1/2}$. So essentially all luminous AGN ($L \gtrsim 10^{42} \text{ erg s}^{-1}$) should exhibit regions in the “clumpy torus” surrounding the AGN, as well as any radiation pressure-driven AGN outflows, which are subject to the super-sonic resonant instability described here. This may provide a natural explanation for clumpiness, velocity sub-structure, and turbulence in the torus (see e.g. Krolik & Begelman 1988; Mason et al. 2006; Sánchez et al. 2006; Nenkova et al. 2008; Thompson

et al. 2009; Mor et al. 2009; Hönig & Kishimoto 2010; Hopkins & Quataert 2010; Hopkins et al. 2012, 2016; Deo et al. 2011), as well as observed time-variability in AGN obscuration (McKernan & Yaqoob 1998; Risaliti et al. 2002). It of course is critical to understand whether this directly alters the AGN-driven winds in the torus region, which will be addressed in future numerical simulations (see e.g. Ciotti & Ostriker 2007; Murray et al. 2005; Elitzur & Shlosman 2006; Miller et al. 2008; Roth et al. 2012; Wada et al. 2009).

As noted before the instability requires only a dust-gas drift velocity, and this can instead be sourced by AGN line-driving of the gas in the narrow/broad line regions. In this case, the scaling of w_s depends on the opacity of the gas, but for plausible values in the narrow-line region, and similar luminosities and densities to those used above, we find comparable or even much larger $w_s \gtrsim 10^2 - 10^5$.

(ii) **Starburst Regions, Radiation-Pressure Driven Winds, and Dust in the ISM around Massive Stars:** Similarly, consider dusty gas in molecular clouds and HII regions surrounding regions with massive stars. It has been widely postulated that radiation pressure on dust (either single-scattering from optical/UV light or multiple-scattering of IR photons) can drive local outflows from these regions (unbinding dense clumps and GMCs and stirring GMC or ISM-scale turbulence).

Assuming geometric absorption of radiation by the dust ($Q_\lambda \sim 1$), a random patch of gas in a GMC (with temperature $T \sim 10 \text{ K}$, density $n \sim n_{10} 10 \text{ cm}^{-3}$) at a distance $R \sim R_{\text{pc}}$ pc from a source with luminosity $L \sim L_{1000} 1000 L_\odot$ has $w_s \sim 10 L_{1000}^{1/2} n_{10}^{-1/2} R_{\text{pc}}^{-1}$. Similarly, consider a GMC of some arbitrary total mass M_{cl} and total size $R \sim R_{10} 10 \text{ pc}$, which has converted a fraction $\sim 0.1 \epsilon_{0.1}$ of its mass into clouds. If we assume a typical mass-to-light ratio for young stellar populations ($\sim 1100 L_\odot / M_\odot$), we find $w_s \sim 10 R_{10}^{1/2} \epsilon_{0.1}^{1/2}$.

So we again expect these instabilities to be important. They may fundamentally alter the ability of radiation pressure from massive stars to drive outflows and source local turbulence (a subject of considerable interest and controversy; see Murray et al. 2005; Thompson et al. 2005; Krumholz et al. 2007; Schartmann et al. 2009; Hopkins et al. 2011, 2013, 2014; Guszejnov et al. 2016; Grudić et al. 2016). They will also directly source dust-to-gas fluctuations, which can in turn drive abundance anomalies in next-generation stars (Hopkins 2014; Hopkins & Conroy 2015), as well as altering the dust growth, chemistry, and cooling physics of the clouds (Goldsmith & Langer 1978; Dopcke et al. 2013; Ji et al. 2014; Chiaki et al. 2014).

(iii) **Cool Star (AGB and Red Giant) Winds and PNe:** In the photospheres and envelopes of cool stars, dust forms and is accelerated by continuum radiation pressure. This contributes to the launching and acceleration of winds, and potentially defines key wind properties, such as their “clumpiness” and variability in time and space. There has been extensive study of accelerating dust-gas mixtures in this context (see references in § 7.1).

Consider an expanding photosphere/wind ($\rho = \dot{M} / (4\pi r^2 v_{\text{wind}})$) with $v_{\text{wind}} \sim v_{10} 10 \text{ km s}^{-1}$, $\dot{M} \sim \dot{M}_{-3} 10^{-3} M_\odot \text{ yr}^{-1}$, and gas temperature $T \sim T_{1000} 1000 \text{ K}$ (in the outflow) around a giant with luminosity $L \sim L_5 10^5 L_\odot$. Assuming geometric absorption, we obtain $w_s \sim 2 (L_5 v_{10} / \dot{M}_{-3} T_{1000})^{1/2}$. We therefore expect $w_s \sim 1$ (but with a broad range, $w_s \sim 0.1 \rightarrow 10$, or larger) for plausible parameters of different cool stars, and different locations of the grains within the photosphere and wind. This places the instability perhaps in the most interesting range, where certain regimes of the outflows (with

$w_s \lesssim 1$, but not vanishingly small) would be subject to the long-wavelength instability, and other regimes (with $w_s \gtrsim 1$) would be subject to the short-wavelength acoustic RDI. The long-wavelength instability, which grows fastest in the direction parallel to \mathbf{w}_s , could perhaps explain large-scale features such as dust “shells” or “arcs” (similar to ideas proposed by Morris 1993; Winters et al. 1994; Deguchi 1997). In contrast, regimes with $w_s \gtrsim 1$, where the fastest-growing modes are short-wavelength and oblique, would likely develop non-linearly into turbulence, seeding clumpy sub-structure in the winds and in emission (a subject of considerable interest; see e.g. Weigelt et al. 1998; Fong et al. 2003; Young et al. 2003; Ziurys et al. 2007; Agúndez et al. 2010; Cox et al. 2012). The latter would almost certainly trigger secondary non-linear instabilities by driving large dust-gas clumping; for example via radiative Rayleigh-Taylor instabilities, dust opacity/self-shielding effects, and dust collisions/growth in the wind.

(iv) **Proto-planetary Disks:** As discussed in § 7, instabilities of the coupled dust-gas system in proto-planetary disks are particularly interesting, given their implications for planet formation and observable disk properties. In proto-planetary disks we expect drift velocities to be highly subsonic. For a disk with parameters following Chiang & Youdin (2010) at radius $r \sim r_{10} 10 \text{ au}$ and surface density $\Sigma \sim \Sigma_{\text{MMSN}} 1000 \text{ g cm}^{-3} (r/\text{au})^{-1.5}$, pebbles with size $R_d \sim R_{d,\text{cm}} \text{ cm}$ will have $w_s \sim 0.005 r_{10}^{25/14} R_{d,\text{cm}} \Sigma_{\text{MMSN}}^{-1}$ (Nakagawa et al. 1986). Since $w_s \ll 1$ we expect the growth rate of the instabilities here to have a maximum value $\Im(\omega) \sim w_s^2 \mu t_s^{-1}$. For plausible disk parameters this is much longer than the radial drift timescale $\sim r/v_{\text{drift}}$ for the grains to drift through the disk.

Given this relatively low growth rate, we do not expect this *particular* sound-wave resonance (the acoustic RDI) to be dominant. However, we *do* expect other examples from the broad class of RDI resonances to be interesting. For example, as noted in SH, the well-studied disk “streaming instability” is an RDI with the disk epicyclic frequency. Other wave families such as convective, slow magnetosonic, and Hall magnetosonic-cyclotron waves are also present with slow phase velocities, which can give rise to much larger growth rates (as compared to the acoustic RDI studied here) when $w_s \ll 1$. These will be studied in future work.

9 CONCLUSIONS

9.1 Summary

We study the acoustic family of the class of “resonant drag instabilities” (RDI) explored in SH. Such instabilities can occur when a relative drift velocity arises between the dust and gas in a coupled dust-gas mixture (due, for example, to different radiative forces on the dust and the gas, or pressure support of the gas). SH studied a general gas system and showed that if the gas (absent dust) supports some undamped waves, a streaming velocity that “resonates with” the wave phase velocity usually creates an instability (the RDI). In this work, we focus on the case where the gas is governed by neutral hydrodynamics and supports sound waves, studying the “acoustic RDI” (resonance with sound waves) and a collection of other non-resonant unstable modes (these are important in certain regimes, e.g., at long-wavelengths or high dust-to-gas ratios). Although neutral hydrodynamics is perhaps the simplest gas system possible, these instabilities have not (to our knowledge) been studied in detail in previous literature, despite their likely relevance for a wide variety of astrophysical systems.

We identify a spectrum of exponentially-growing linear instabilities which *directly* source fluctuations in the dust-to-gas ratio.

Under certain conditions *all* wavelengths feature unstable modes, some of which have growth rates that increase without limit with increasing wavenumber. We show that the qualitative behavior is not sensitive to the gas equation-of-state, the form of the drag law (constant drag coefficient, Epstein, Stokes, or Coulomb drag), the dust-to-gas ratio, or other details. We derive stability conditions and simple closed analytic expressions for the growth rates of the instability (§ 3) in a variety of astrophysically relevant regimes.

There is one critical dimensionless parameter that determines the system’s qualitative behavior, viz., ratio of the mean dust drift velocity ($|\mathbf{v}_{\text{dust}} - \mathbf{u}_{\text{gas}}|^{\text{drift}}$) to the gas sound speed c_s :

$$w_s \equiv \frac{|\mathbf{w}_s|}{c_s} = \frac{|\mathbf{v}_{\text{dust}} - \mathbf{u}_{\text{gas}}|^{\text{drift}}}{c_s} = \frac{|\Delta \mathbf{a}_{\text{dust-gas}}(t_s(\mathbf{a}, \rho, \dots))}{c_s(1 + \mu)}. \quad (32)$$

Here, the drift velocity \mathbf{w}_s is the “terminal” velocity when the dust and gas experience accelerations which differ by some amount $\Delta \mathbf{a}_{\text{dust-gas}}$, t_s is the drag coefficient or “stopping time” (determined by the drag law), and μ is the dust-to-gas mass ratio.

When $w_s \geq 1$, i.e. when the dust is moving supersonically relative to the gas, the system is strongly unstable at *all* wavelengths. There are multiple unstable modes but the acoustic RDI from SH (§ 3.7.1) is the most rapidly growing. The growth rate $\Im(\omega)$ increases *without limit* with increasing wavenumber k as $\Im(\omega) \sim (\mu k c_s / t_s)^{1/2}$ (in a mid range of k) or $\Im(\omega) \sim (\mu k c_s / t_s^2)^{1/3}$ (at high k), independent of w_s . These modes propagate at a critical angle $\cos \theta = \pm 1/w_s$ with respect to the drift direction; the wavespeed is the normal sound speed, and the drift velocity along the wavevector $\hat{\mathbf{k}}$ exactly matches this, allowing the dust to coherently push gas, and generate density perturbations. The denser gas then decelerates the dust further, causing a pileup, which runs away. For modes at angles that do not match the resonance condition ($\cos \theta \neq \pm 1/w_s$), the growth rates saturate at finite values (i.e., $\Im(\omega)$ does not increase indefinitely with k).

When $w_s < 1$, i.e. when the dust is moving subsonically relative to the gas, the resonance above does not exist but there are still unstable, long-wavelength modes whose growth rate peaks or saturates above some wavenumber $k \propto w_s$, with maximum growth rate $\Im(\omega) \sim w_s^2 \mu / t_s$.

9.2 Implications, Caveats, & Future Work

In all cases, the instabilities drive dust-gas segregation and local fluctuations in the dust-to-gas ratio, compressible fluctuations in the gas density and velocity, and clumping within the dust (§ 3.9). Non-linearly, we expect them to saturate by breaking up into turbulent motions (in both dust and gas) which can be subsonic or supersonic, and in both cases can give rise to large separations between dense gas-dominated and dust-dominated regions. We provide simple estimates for the saturated turbulent amplitude (§ 5).

We discuss some astrophysical implications of these instabilities (§ 8) and argue that the “resonant” instability is likely to be important in the dusty gas around AGN (in the torus or narrow-line regions), starbursts, giant molecular clouds and other massive-star forming regions, where $w_s \gg 1$ almost everywhere. In the winds and photospheres of cool stars, simple estimates suggest $w_s \sim 1$, with a broad range depending on the local conditions and location in the atmosphere. Thus, we again expect these instabilities to be important. In each of these regimes, the instability may fundamentally alter the ability of the system to drive winds via radiation pressure (on the dust or the gas), and will source turbulence, velocity sub-structure, clumping, and potentially observable inhomogeneities in the winds.

More detailed conclusions will require detailed numerical

simulations to study the non-linear evolution of these systems. Our analytic results here make it clear what physics must be included to study such instabilities – in particular, physical drag laws (with realistic density and velocity dependence) and backreaction from the dust to the gas – and the range of scales that must be resolved. Most previous studies of such systems either did not include the appropriate drag physics or lacked the resolution to treat these modes properly. This is especially challenging for the resonant mode: because the growth rate increases without limit at high k , it could (in principle) become more important and grow ever-faster as the simulation resolution increases.

We have focused on a relatively simple case here, namely gas with a pure acoustic wave in the absence of dust. This ignores, for example, magnetic fields, which alter the mode structure and could influence the grain “drag” directly (if the grains are charged). As shown in SH, the RDI generically exists for systems that support undamped linear waves, so we expect a similar rich phenomenology of instabilities (both resonant and non-resonant) in other systems. However it is outside the scope of this work to explore these in detail.

Another topic which we will explore in more detail is the influence of a broad size spectrum of dust grains. This is discussed in § 2.3.2, where we argue that under most conditions, we can think of the results of this work as being relevant for the large grains (specifically, the largest grains which contain a large fraction of the grain mass), because these dominate the mass and back-reaction on the gas. However as shown there, under some circumstances there is a complicated mix of terms dominated by small grains and others dominated by large grains, which could couple indirectly. Moreover, because the RDI can resonate with any wave family, it is possible that (for example) small, tightly-coupled grains (which may be more stable if considered in isolation) generate wave families to which larger grains can couple via the RDI (or vice versa).

ACKNOWLEDGMENTS

We would like to thank E. S. Phinney and E. Quataert for helpful discussions. Support for PFH & JS was provided by an Alfred P. Sloan Research Fellowship, NASA ATP Grant NNX14AH35G, and NSF Collaborative Research Grant #1411920 and CAREER grant #1455342. JS was funded in part by the Gordon and Betty Moore Foundation through Grant GBMF5076 to Lars Bildsten, Eliot Quataert and E. Sterl Phinney.

REFERENCES

- Agúndez, M., Cernicharo, J., & Guélin, M. 2010, *ApJL*, 724, L133
- Bai, X.-N., & Stone, J. M. 2010a, *ApJS*, 190, 297
- . 2010b, *ApJL*, 722, L220
- Bell, A. R. 2004, *MNRAS*, 353, 550
- Berruyer, N. 1991, *A&A*, 249, 181
- Bracco, A., Chavanis, P. H., Provenzale, A., & Spiegel, E. A. 1999, *Physics of Fluids*, 11, 2280
- Carballido, A., Stone, J. M., & Turner, N. J. 2008, *MNRAS*, 386, 145
- Chiaki, G., Schneider, R., Nozawa, T., Omukai, K., Limongi, M., Yoshida, N., & Chieffi, A. 2014, *MNRAS*, 439, 3121
- Chiang, E., & Youdin, A. N. 2010, *Annual Review of Earth and Planetary Sciences*, 38, 493
- Ciotti, L., & Ostriker, J. P. 2007, *ApJ*, 665, 1038
- Clair, B. P. L., Hamielec, A. E., & Pruppacher, H. R. 1970, *J. Atmos. Sci.*, 27, 308
- Cochran, W. D., & Ostriker, J. P. 1977, *ApJ*, 211, 392
- Cox, N. L. J., et al. 2012, *A&A*, 537, A35
- Cuzzi, J. N., Hogan, R. C., Paque, J. M., & Dobrovolskis, A. R. 2001, *ApJ*, 546, 496
- Davis, S. W., Jiang, Y.-F., Stone, J. M., & Murray, N. 2014, *ApJ*, in press, arXiv:1403.1874
- Deguchi, S. 1997, in *IAU Symposium*, Vol. 180, *Planetary Nebulae*, ed. H. J. Habing & H. J. G. L. M. Lamers, 151
- Deo, R. P., Richards, G. T., Nikutta, R., Elitzur, M., Gallagher, S. C., Ivezić, Ž., & Hines, D. 2011, *ApJ*, 729, 108
- Dittrich, K., Klahr, H., & Johansen, A. 2013, *ApJ*, 763, 117
- Dopcke, G., Glover, S. C. O., Clark, P. C., & Klessen, R. S. 2013, *ApJ*, 766, 103
- Draine, B. T. 2003, *ARA&A*, 41, 241
- Draine, B. T., & Salpeter, E. E. 1979, *ApJ*, 231, 77
- Elitzur, M., & Shlosman, I. 2006, *ApJL*, 648, L101
- Fong, D., Meixner, M., & Shah, R. Y. 2003, *ApJL*, 582, L39
- Goldsmith, P. F., & Langer, W. D. 1978, *ApJ*, 222, 881
- Grudić, M. Y., Hopkins, P. F., Faucher-Giguère, C.-A., Quataert, E., Murray, N., & Kereš, D. 2016, *MNRAS*, in press, arXiv:1612.05635
- Guszejnov, D., Krumholz, M. R., & Hopkins, P. F. 2016, *MNRAS*, 458, 673
- Hartquist, T. W., & Havnes, O. 1994, *Astrophysics and Space Science*, 218, 23
- Heckman, T. M., Armus, L., & Miley, G. K. 1990, *ApJS*, 74, 833
- Hönig, S. F., & Kishimoto, M. 2010, *A&A*, 523, A27
- Hopkins, P. F. 2014, *ApJ*, 797, 59
- . 2016, *MNRAS*, 456, 2383
- Hopkins, P. F., & Conroy, C. 2015, *ApJ*, in press, arXiv:1512.03834
- Hopkins, P. F., & Elvis, M. 2010, *MNRAS*, 401, 7
- Hopkins, P. F., Hayward, C. C., Narayanan, D., & Hernquist, L. 2012, *MNRAS*, 420, 320
- Hopkins, P. F., Keres, D., Onorbe, J., Faucher-Giguere, C.-A., Quataert, E., Murray, N., & Bullock, J. S. 2014, *MNRAS*, 445, 581
- Hopkins, P. F., & Lee, H. 2016, *MNRAS*, 456, 4174
- Hopkins, P. F., Narayanan, D., Murray, N., & Quataert, E. 2013, *MNRAS*, 433, 69
- Hopkins, P. F., & Quataert, E. 2010, *MNRAS*, 405, L41
- Hopkins, P. F., Quataert, E., & Murray, N. 2011, *MNRAS*, 417, 950
- Hopkins, P. F., Torrey, P., Faucher-Giguère, C.-A., Quataert, E., & Murray, N. 2016, *MNRAS*, 458, 816
- Jacquet, E., Balbus, S., & Latter, H. 2011, *MNRAS*, 415, 3591
- Jalali, M. A. 2013, *ApJ*, in press, arxiv:1301.2064
- Ji, A. P., Frebel, A., & Bromm, V. 2014, *ApJ*, 782, 95
- Johansen, A., & Youdin, A. 2007, *ApJ*, 662, 627
- Krolik, J. H., & Begelman, M. C. 1988, *ApJ*, 329, 702
- Krumholz, M. R., Klein, R. I., & McKee, C. F. 2007, *ApJ*, 656, 959
- Krumholz, M. R., & Matzner, C. D. 2009, *ApJ*, 703, 1352
- Krumholz, M. R., & Thompson, T. A. 2012, *ApJ*, 760, 155
- Kuiper, R., Klahr, H., Beuther, H., & Henning, T. 2012, *A&A*, 537, A122
- Kulsrud, R., & Pearce, W. P. 1969, *ApJ*, 156, 445
- Lee, H., Hopkins, P. F., & Squire, J. 2016, *MNRAS*, in press, arXiv:1612.05264
- MacGregor, K. B., & Stencel, R. E. 1992, *ApJ*, 397, 644
- Mason, R. E., Geballe, T. R., Packham, C., Levenson, N. A., Elitzur, M., Fisher, R. S., & Perlman, E. 2006, *ApJ*, 640, 612
- Mastrodomos, N., Morris, M., & Castor, J. 1996, *ApJ*, 468, 851

Mathis, J. S., Rumpl, W., & Nordsieck, K. H. 1977, *ApJ*, 217, 425
 Matthews, J. H., Bell, A. R., Blundell, K. M., & Araudo, A. T. 2017, *MNRAS*, 469, 1849
 McKernan, B., & Yaqoob, T. 1998, *ApJL*, 501, L29+
 Miller, L., Turner, T. J., & Reeves, J. N. 2008, *A&A*, 483, 437
 Monceau-Baroux, R., & Keppens, R. 2017, *A&A*, 600, A134
 Mor, R., Netzer, H., & Elitzur, M. 2009, *ApJ*, 705, 298
 Morris, M. 1993, in *European Southern Observatory Conference and Workshop Proceedings*, Vol. 46, European Southern Observatory Conference and Workshop Proceedings, ed. H. E. Schwarz, 60
 Murray, N., Quataert, E., & Thompson, T. A. 2005, *ApJ*, 618, 569
 —. 2010, *ApJ*, 709, 191
 Nakagawa, Y., Sekiya, M., & Hayashi, C. 1986, *Icarus*, 67, 375
 Nenkova, M., Sirocky, M. M., Ivezić, Ž., & Elitzur, M. 2008, *ApJ*, 685, 147
 Pan, L., Padoan, P., Scalo, J., Kritsuk, A. G., & Norman, M. L. 2011, *ApJ*, 740, 6
 Riquelme, M. A., & Spitkovsky, A. 2009, *ApJ*, 694, 626
 Risaliti, G., Elvis, M., & Nicastro, F. 2002, *ApJ*, 571, 234
 Roth, N., Kasen, D., Hopkins, P. F., & Quataert, E. 2012, *ApJ*, 759, 36
 Sánchez, F. M., Davies, R. I., Eisenhauer, F., Tacconi, L. J., Genzel, R., & Sternberg, A. 2006, *A&A*, 454, 481
 Sandford, II, M. T., Whitaker, R. W., & Klein, R. I. 1984, *ApJ*, 282, 178
 Sandin, C., & Höfner, S. 2003, *A&A*, 404, 789
 Schartmann, M., Meisenheimer, K., Klahr, H., Camenzind, M., Wolf, S., & Henning, T. 2009, *MNRAS*, 393, 759
 Scoville, N. Z., Polletta, M., Ewald, S., Stolovy, S. R., Thompson, R., & Rieke, M. 2001, *AJ*, 122, 3017
 Simis, Y. J. W., Icke, V., & Dominik, C. 2001, *A&A*, 371, 205
 Soker, N. 2000, *ApJ*, 540, 436
 —. 2002, *ApJ*, 570, 369
 Squire, J., & Hopkins, P. F. 2017, *Physical Review Letters*, in press, arXiv:1706.05020
 Thompson, G. D., Levenson, N. A., Uddin, S. A., & Sirocky, M. M. 2009, *ApJ*, 697, 182
 Thompson, T. A., Quataert, E., & Murray, N. 2005, *ApJ*, 630, 167
 Tytarenko, P. V., Williams, R. J. R., & Falle, S. A. E. G. 2002, *MNRAS*, 337, 117
 Wada, K., Papadopoulos, P., & Spaans, M. 2009, *ApJ*, in press, arXiv:0906.5444
 Wardle, M. 1990, *MNRAS*, 246, 98
 Weigelt, G., Balega, Y., Bloecker, T., Fleischer, A. J., Osterbart, R., & Winters, J. M. 1998, *A&A*, 333, L51
 Winters, J. M., Dominik, C., & Sedlmayr, E. 1994, *A&A*, 288, 255
 Wise, J. H., Abel, T., Turk, M. J., Norman, M. L., & Smith, B. D. 2012, *MNRAS*, 427, 311
 Woitke, P. 2006a, *A&A*, 452, 537
 —. 2006b, *A&A*, 460, L9
 Youdin, A. N., & Goodman, J. 2005, *ApJ*, 620, 459
 Young, P. A., Highberger, J. L., Arnett, D., & Ziurys, L. M. 2003, *ApJL*, 597, L53
 Ziurys, L. M., Milam, S. N., Apponi, A. J., & Woolf, N. J. 2007, *Nature*, 447, 1094

APPENDIX A: RELATION TO THE MATRIX FORMALISM OF SQUIRE & HOPKINS (2017)

Throughout the main text, our analysis was carried out through asymptotic expansions of the dispersion relation, so as to allow investigation into non-resonant modes (e.g., for $|\mathbf{w}_s| < c_s$, and the “long-wavelength” modes). To clarify the link to the RDI derivation in SH, in this appendix, we calculate the acoustic RDI growth rates using the Jordan-form perturbation theory formalism of SH. We use the dimensionless variables of § 3 (Eq. (7)), and, for the sake of concreteness, set $\hat{\mathbf{w}}_s = \hat{\mathbf{z}}$ and $\hat{\mathbf{k}}_{\perp} = \hat{\mathbf{x}}$ (it was not necessary to choose a specific direction in derivation of the dispersion relation, Eq. (8)). We also ignore u_y and v_y because these are decoupled from the sound-wave eigenmodes (these propagate in the $\hat{\mathbf{k}}$ direction).

From Eq. (3), the coupled dust-gas equations are

$$\omega \boldsymbol{\xi} = \begin{pmatrix} \kappa_{\parallel} & \mathbf{k}^T & 0 \\ 0 & \kappa_{\parallel} I + D_{\text{drag}} & C_v \\ \mu T_{\rho_d}^{(1)} & \mu T_v^{(1)} & \mathcal{F} + \mu T_g^{(1)} \end{pmatrix} \boldsymbol{\xi}, \quad (\text{A1})$$

where $\boldsymbol{\xi} = (\delta\rho_d, \delta v_x, \delta v_z, \delta\rho, \delta u_x, \delta u_z)^T$, $\mathbf{k}^T = (k_x, k_z)$, $T_{\rho_d}^{(1)} = (0, 0, i w_s)^T$, $T_v^{(1)}$ and $T_g^{(1)}$ are not needed,

$$D_{\text{drag}} = \begin{pmatrix} -i & 0 \\ 0 & -i\tilde{\zeta} \end{pmatrix}, \quad C_v = \begin{pmatrix} 0 & i & 0 \\ -i w_s \eta & 0 & -i\tilde{\zeta} \end{pmatrix}, \quad (\text{A2})$$

and

$$\mathcal{F} = \begin{pmatrix} 0 & k_x & k_z \\ k_x & 0 & 0 \\ k_z & 0 & 0 \end{pmatrix}. \quad (\text{A3})$$

When at resonance, i.e. $\kappa_{\parallel} = \mathbf{k} \cdot \mathbf{w}_s = k$ (where $\omega = k$ is forward-propagating sound-wave eigenvalue of \mathcal{F}), the matrix in Eq. (A1) is defective. This means that although $\omega = \kappa_{\parallel}$ has multiplicity 2, it has only one associated eigenvector. This creates an RDI, the growth rate of which scales as $\sim \mu^{1/2}$ because the matrix is singular (rather than $\sim \mu$ as for standard perturbation theory). From SH (their Eq. 10), the perturbed eigenvalues in the “mid- k ” regime (before \mathbf{k}^T dominates over D_{drag} in Eq. (A1)) are

$$\omega = \kappa_{\parallel} \pm i \mu^{1/2} \left[(\boldsymbol{\xi}_{\mathcal{F}}^L T_{\rho_d}^{(1)}) (\mathbf{k}^T D_{\text{drag}}^{-1} C_v \boldsymbol{\xi}_{\mathcal{F}}^R) \right]^{1/2} + \mathcal{O}(\mu) \quad (\text{A4})$$

Here

$$\boldsymbol{\xi}_{\mathcal{F}}^L = \frac{1}{\sqrt{2k}} \begin{pmatrix} k & k_x & k_z \end{pmatrix}, \quad \boldsymbol{\xi}_{\mathcal{F}}^R = \frac{1}{\sqrt{2k}} \begin{pmatrix} k \\ k_x \\ k_z \end{pmatrix} \quad (\text{A5})$$

are the right and left eigenvectors of the (forward-propagating) sound wave. Equation (A4) is easily verified to be the same as Eq. (16) from the main text, up to $\mathcal{O}(\mu^{1/2})$.

In the “high- k ” regime, the eigenvalue $\omega = \kappa_{\parallel}$ is nearly triply defective (meaning it has multiplicity 3 with one associated eigenvector), because $\mathbf{k}^T \gg D_{\text{drag}}$. The perturbed eigenvalue is then

$$\omega = \kappa_{\parallel} + \mu^{1/3} \left[(\boldsymbol{\xi}_{\mathcal{F}}^L T_{\rho_d}^{(1)}) (\mathbf{k}^T C_v \boldsymbol{\xi}_{\mathcal{F}}^R) \right]^{1/3} + \mathcal{O}(\mu^{2/3}), \quad (\text{A6})$$

which matches Eq. (17) from the main text.

We cannot treat the “long-wavelength” instability (Sec. 3.4) using this method, because $\mu \gtrsim \kappa_{\parallel}$ in this regime. In other words, $\mu T_{\rho_d}^{(1)}$, $\mu T_v^{(1)}$, and $\mu T_g^{(1)}$ are no longer a small perturbation to the fluid, and there is no well-defined undamped sound wave with which the dust can resonate (see § 3.9 and Fig. 2 for further discussion). The long-wavelength growth rate Eq. (10) can be derived

from the matrix (A1) by treating κ_{\parallel} and \mathcal{F} as a small perturbation to D_{drag} , $C_{\mathbf{v}}$ and $T^{(1)}$ (i.e., assuming small k). However, the procedure is not particularly illuminating (or, for that matter, easier algebraically than using the dispersion relation), so we do not reproduce it here.